Transcriptional profiling reveals TRPM5-expressing cells involved in viral infection in the olfactory epithelium

B. Dnate' Baxter[1,2,‡], Eric D. Larson[3 ‡], Paul Feinstein[4], Arianna Gentile Polese[1,2], Andrew N. Bubak[5], Christy S. Niemeyer[5], Laetitia Merle[1,2], Doug Shepherd[6], Vijay R. Ramakrishnan[3], Maria A. Nagel[5], and Diego Restrepo[1,2,*]

[1]Neuroscience Graduate Program, University of Colorado Anschutz Medical Campus, Aurora, CO 80045, USA

[2]Department of Cell and Developmental Biology, University of Colorado Anschutz Medical Campus, Aurora, CO 80045, USA

[3]Department of Otolaryngology, University of Colorado Anschutz Medical Campus, Aurora, CO 80045, USA

[4]Department of Biological Sciences, Hunter College, CUNY, New York, NY, 10065, USA

[5]Department of Neurology, University of Colorado Anschutz Medical Campus, Aurora, CO 80045, USA

[6]Department of Pharmacology, University of Colorado Anschutz Medical Campus and Center for Biological Physics and Department of Physics, Arizona State University, USA

[‡]Co-first authors

[*]Corresponding author: Diego Restrepo, diego.restrepo@cuanschutz.edu

Understanding viral infection of the olfactory epithelium is essential because smell loss can occur with coronavirus disease 2019 (COVID-19), caused by severe acute respiratory syndrome coronavirus clade 2 (SARS-CoV-2), and because the olfactory nerve is an important route of entry for viruses to the central nervous system. Specialized chemosensory epithelial cells that express the transient receptor potential cation channel subfamily M member 5 (TRPM5) are found throughout the airways and intestinal epithelium and are involved in responses to viral infection. Herein we performed deep transcriptional profiling of olfactory epithelial cells sorted by flow cytometry based on the expression of fluorescent protein markers for olfactory sensory neurons and TRPM5. We find profuse expression of transcripts involved in inflammation, immunity and viral infection in TRPM5-expressing microvillous cells and olfactory sensory neurons. These cells express the *Tmprss2* transcript that encodes for a serine protease that primes the SARS-CoV-2 spike protein before entry into host cells. Our study provides new insights into a potential role for TRPM5-expressing cells in viral infection of the olfactory epithelium.

38 Self-reported loss of smell in a large fraction of patients with coronavirus disease 2019 (COVID-
39 19), caused by severe acute respiratory syndrome coronavirus clade 2 (SARS-CoV-2),
40 (Giacomelli et al., 2020; Parma et al., 2020; Yan et al., 2020a; Yan et al., 2020b) raises the
41 question of how SARS-CoV-2 affects olfaction in a subset of patients. Entry of SARS-CoV-2
42 into cells is mediated by spike protein attachment to the SARS-CoV receptor ACE2 followed by
43 spike protein priming by the serine protease TMPRSS2 (Hoffmann et al., 2020). Chemosensory
44 cells found in the airway (SCCs/brush cells) and intestinal epithelium (tuft cells) express the
45 transient receptor potential cation channel subfamily M member 5 (TRPM5) and other elements
46 of the taste transduction pathway and have been implicated in immune and inflammatory
47 responses to bacterial, viral and parasitic infection (Luo et al., 2019; Maina et al., 2018; O'Leary
48 et al., 2019; Perniss et al., 2020; Rane et al., 2019; Saunders et al., 2014; Tizzano et al., 2010). In
49 the olfactory epithelium TRPM5 and other proteins involved in taste transduction are also
50 expressed in SCC-like microvillous cells (MVCs)(Genovese and Tizzano, 2018; Lin et al.,
51 2008), which have been proposed to be involved in a protective response to high concentrations
52 of odorants (Fu et al., 2018; Lemons et al., 2017). The ACE2 receptor and TMPRSS2 are
53 expressed in support cells, stem cells, and MVCs (Brann et al., 2020; Fodoulian et al., 2020).
54 However, whether MVCs play a role in viral infection or viral infection defense of the olfactory
55 epithelium is unknown.
56
57 Herein, we performed transcriptional profiling of MVCs and a subset of olfactory sensory
58 neurons (OSNs) expressing eGFP under control of the TRPM5 promoter (OSN_eGFP+
59 cells)(Lin et al., 2007; Lopez et al., 2014). In order to profile these low abundance cells we used
60 a modified version of Probe-Seq, which allows deep transcriptional profiling of specific cell

61 types identified by fluorescent markers as the defining feature (Amamoto et al., 2019). We
62 crossed a mouse expressing mCherry in the nuclei of OSNs under control of the OMP promoter
63 (OMP-H2B::mCherry mice) with TRPM5-eGFP transgenic mice (Clapp et al., 2006) (OMP-
64 H2B::mCherry/TRPM5-eGFP mice). We isolated cells from the olfactory epithelium and used
65 fluorescence-activated cell sorting (FACS) to sort MVC_eGFP cells (mCherry negative and
66 eGFP positive) and cells labeled by OMP-driven mCherry that did or did not express eGFP
67 (OSN_eGFP+ and OSN_eGFP- cells) followed by transcriptional profiling by RNA sequencing
68 (RNAseq).
69
70

71 **Results**

72

73 **Fluorescence-activated cell sorting of cells isolated from the main olfactory epithelium.** The
74 olfactory epithelium of OMP-H2B::mCherry/TRPM5-eGFP mice expressed nuclear mCherry
75 driven by the OMP promoter in the intermediate layer of the olfactory epithelium (Figures 1a), as
76 expected for the location of nuclei of mature OSNs (Farbman and Margolis, 1980). eGFP
77 expression driven by the TRPM5 promoter was found in MVCs, with cell bodies located mostly
78 in the apical layer of the epithelium (asterisks), and at lower expression levels in a subset of
79 OSNs double-labeled with mCherry (Figure 1a), consistent with earlier publications (Lin et al.,
80 2008; Lin et al., 2007; Pyrski et al., 2017).

81

82 We proceeded to isolate cells from the main olfactory epithelium of OMP-
83 H2B::mCherry/TRPM5-eGFP mice (see Methods, Figure 1b). Figure 1c shows two isolated
84 OSNs with differential expression of eGFP. Using flow cytometry we found that fluorescence
85 intensity of individual cells for mCherry and eGFP spanned several orders of magnitude (Figure
86 1d). We proceeded to sort three groups of cells: high mCherry-expressing cells with low and
87 high eGFP fluorescence (presumably mature OSNs, these cells are termed OSN_eGFP- and
88 OSN_eGFP+ cells respectively) and cells with low mCherry and high eGFP expression
89 (MVC_eGFP, presumably MVCs). Reverse transcription quantitative PCR (RT-qPCR) showed
90 that, as expected the OSN_eGFP- and OSN_eGFP+ cells have higher levels of OMP transcript
91 than MVC_eGFP cells (Figure 1e,i), and OSN_eGFP+ cells and MVC_eGFP cells have higher
92 levels of eGFP transcript compared to OSN_eGFP- cells (Figure 1e,ii). Furthermore, compared
93 to OSN_eGFP- cells both the MVC_eGFP cells and OSN_eGFP+ cells expressed higher levels

94 of TRPM5 transcript (Figure 1e,iii) and choline acetyl transferase (ChAT)(Figure 1e,iv), a
95 protein involved in acetylcholine neurotransmission that is expressed in MVCs (Ogura et al.,
96 2011). The asterisks in Figure 1e denote significant differences tested with either t-test or
97 ranksum with p-values below the p-value of significance corrected for multiple comparisons
98 using the false discovery rate (pFDR)(Curran-Everett, 2000) (pFDR is 0.033 for OMP, 0.05 for
99 TRPM5, 0.05 for EGFP and 0.03 for ChAT, n=8 for OMP OSN_eGFP-, 4 for OMP
100 OSN_eGFP+ and 4 for MVC_eGFP cells).
101
102 **The number of OSN_eGFP+ cells sorted by FACS is decreased when OMP-**
103 **H2B::mCherry/TRPM5-eGFP mice are placed in ventilated cages.** In our vivarium we have
104 ventilated cages (HV cages) where air is mechanically exchanged with fresh air once every
105 minute and static cages (LV cages) where air is exchanged passively through a filter in the cover.
106 When we moved the OMP-H2B::mCherry/TRPM5-eGFP to HV cages we noticed a decrease in
107 the number of OSN_eGFP+ cells sorted per mouse (Figures 2a,b and c), suggesting that changes
108 in ventilation conditions affect TRPM5 promoter-driven expression of eGFP. Following this
109 observation, mice were moved back to LV cages. We proceeded to study the dependence of the
110 number of OSN_eGFP+ cells sorted on the number of days in LV vs. HV cages. The number of
111 OSN_eGFP+ cells is positively correlated with the number of days the animal spends in LV
112 cages (Figure 2d) and negatively correlated to the number of days the animals spend in the HV
113 cages (Figure 2e). Generalized linear model (GLM) analysis found significant differences for the
114 number of OSN_eGFP+ cells sorted as a function of the number of days in LV cages ($p<0.05$, 26
115 observations, 24 d.f., F-statistic = 5.64, p-value for GLM <0.05) and the number of days in HV
116 cages ($p<0.05$, 26 observations, 24 d.f., F-statistic = 5.99, p-value for GLM <0.05). For RNAseq

117 experiments one FACS sort was done using cells from mice born and maintained in HV housing,
118 and the OSN_eGFP+ yield was low. Subsequently, we performed all FACS with cells isolated
119 from the olfactory epithelium of mice raised in LV cages.
120
121 **Coverage of TRPM5 transcript by RNAseq encompasses the full transcript in MVC_eGFP**
122 **cells and OSN_eGFP+ cells.** Pyrski and co-workers did not find full-length TRPM5 transcript
123 in reverse transcriptase polymerase chain reactions with mRNA extracted from isolated OSNs
124 from the adult mouse and did not find *in situ* signal in the OSN layer of the olfactory epithelium
125 for the full-length TRPM5 transcript (Pyrski et al., 2017). These investigators found full-length
126 TRPM5 transcript and strong *in situ* signal in MVCs. We find strong *in situ* signal for TRPM5 in
127 MVC_eGFP cells located in the apical layer of the olfactory epithelium (Figure 3aii, asterisks).
128 In addition, we find sparse TRPM5 *in situ* labeling in the nuclear OSN layer (Figure 3aii,
129 arrows). In order to gain a better understanding of which TRPM5 transcript is expressed in OSNs
130 we performed an analysis of TRPM5 transcript coverage for the RNAseq performed with RNA
131 from the different groups of cells sorted by FACS. Consistent with *in situ* labeling, TRPM5
132 transcript was significantly higher in OSN_eGFP+ cells compared to OSN_eGFP- cells and in
133 MVC_eGFP cells compared to OSN_eGFP- cells in both male and female adult mice (Figures
134 3b,c). To explore RNA sequencing coverage of individual *Trpm5* exons, we computed read
135 depth over the sequence of the *Trpm5* gene for each sample. We found coverage for all exons in
136 OSN_eGFP+ cells and for all exons except exon 1 and 5'UTR1 in MVC_eGFP cells, but there
137 was no coverage in OSN_eGFP- cells (Figures 3b,c). GLM analysis found statistically
138 significant differences for exons ($p<0.001$, 450 observations, 446 d.f., F-statistic = 33.8, p-value
139 for GLM <0.001), but no overall significance between MVC and OSN_eGFP+ groups ($p>0.05$,

140 450 observations, 446 d.f., F-statistic = 33.8, p-value for GLM <0.001). However, post-hoc
141 ranksum tests did yield significant differences between MVC and OSN_eGFP+ groups for exon
142 1 and 5'UTR1 (p<pFDR=0.0033). We observed no differences in coverage between male and
143 female mice (within MVC_eGFP cells: p>0.05, 210 observations, 206 d.f., F-statistic = 22.8, p
144 value for GLM <0.001; within OSN_GFP+: p>0.05, 240 observations, 236 d.f., F-statistic =
145 11.5, p value for GLM <0.001). Together, these data suggest that both OSN_eGFP+ cells and
146 MVC_eGFP cells are capable of expressing full-length TRPM5 transcript.
147
148 **RNAseq indicates that OSN_eGFP+, OSN_eGFP- and MVC are three distinct groups of**
149 **chemosensory cells in the mouse olfactory epithelium.** Differential gene expression analysis of
150 the RNAseq data was used to compare the three olfactory epithelium cell groups sorted by
151 FACS. We found that expression of 2000 genes was significantly higher in OSN_eGFP+
152 compared to OSN_eGFP-, and expression of 1821 genes was lower in OSN_eGFP+ cells (Figure
153 4 -figure supplement 1 shows the results of RNAseq and Figure 4 -figure supplement 2 shows
154 the metadata). Figure 4a shows expression levels for the transcripts that showed the largest
155 differences between OSN_eGFP+ and OSN_eGFP- cells. The transcripts for TRPM5 and eGFP
156 were among the top 10 genes whose transcription was higher in OSN_eGFP+ compared to
157 OSN_eGFP- with 105-fold and 42-fold increases respectively. This top 10 OSN_eGFP+
158 upregulated group also includes *Avil* and *Adgrg6* that are involved in remodeling processes after
159 peripheral nerve injury (Chuang et al., 2018; Jablonka-Shariff et al., 2020) and *Espn*, encoding
160 for espin, a protein playing a structural role in microvilli of chemosensory cells (Sekerkova et al.,
161 2004). Interestingly, the olfactory activity-dependent protein S100a5 (Fischl et al., 2014) is
162 found among the top 10 OSN_eGFP+ downregulated transcripts suggesting that in these mice

163 the OSN_eGFP+ are not stimulated by the odorants in their housing environment (Figure 4a).
164 Additionally, a majority of the olfactory receptors show decreased transcription in OSN_eGFP+
165 compared to OSN_eGFP- cells (Figures 4a,b) and the volcano plot for olfactory receptor
166 transcript expression shows only 25 olfactory receptors show increased expression in
167 OSN_eGFP+ cells (Figure 4c, based on fold change > 4 and average expression > 100 counts,
168 Table 1).
169
170 Expression of 4386 genes was significantly higher in MVC_eGFP cells compared to
171 OSN_eGFP- cells, and expression of 5630 genes was lower in MVC_eGFP cells (Figure 5 –
172 figure supplement 1). Transcripts for 550 olfactory receptors were lower in MVC_eGFP cells
173 (Figure 5 – figure supplement 1), and no olfactory receptors were upregulated in MVC_eGFP
174 cells compared to OSN_eGFP-. Figure 5a shows expression levels for the transcripts with the
175 largest differences between MVC_eGFP cells and OSN_eGFP- cells. Six of the transcripts that
176 are within the top 10 upregulated genes found in MVC_eGFP cells compared to OSN_eGFP-
177 cells (Figure 5a) are also found within the 10 top upregulated transcripts when OSN_eGFP+ cells
178 are compared to OSN_eGFP- cells (Figure 4a)(*Adgrg6*, *Avi*l, *Cd24a*, *eGFP*, *Espn* and *Trpm5*).
179 TRPM5 and eEGFP were among the top 10 genes whose transcription was higher in
180 MVC_eGFP cells compared to OSN_eGFP- cells with 1471-fold and 75-fold differences
181 respectively. Interestingly, *Pou2f3*, a transcription factor important in differentiation of MVCs
182 (Yamaguchi et al., 2014; Yamashita et al., 2017), is found within the top 10 upregulated genes
183 found in MVC_eGFP cells compared to OSN_eGFP- (Figure 5a) and is also significantly higher
184 in OSN_eGFP+ cells compared to OSN_eGFP- cells (Figure 5 – figure supplement 1). Finally,
185 *OMP* and *s100a5*, genes for two proteins expressed in mature OSNs (Farbman and Margolis,

186 1980; Fischl et al., 2014), were among the top 10 downregulated transcripts in MVC_eGFP cells
187 compared to OSN_eGFP- cells (Figure 5a).
188
189 We found expression of 3068 genes which was significantly higher in MVC_eGFP cells
190 compared to OSN_eGFP+ cells, and expression of 4060 genes was lower in MVC_eGFP cells
191 (Figure 5 – figure supplement 2). Figure 5b shows expression levels for the genes that showed
192 the largest differences between MVC and OSN_eGFP+ cells. Among the 10 genes that are
193 highly expressed in OSN_eGFP+ cells compared to MVC_eGFP cells we find *Pde4a,* a gene
194 expressed in mature OSNs (Juilfs et al., 1997) (*OMP* is also significantly higher in OSN_eGFP+
195 cells, but is not among the top 10 genes, Figure 5 – figure supplement 2). Interestingly, *Hcn2*, a
196 gene that encodes for a hyperpolarization-activated cAMP channel that has been postulated to
197 participate in OSN axon growth and glomerular innervation (Mobley et al., 2010), is found in the
198 top 10 upregulated OSN_eGFP+ genes. Finally, the gene encoding for the synaptic protein
199 Snap25 is found in the top 10 upregulated lists for both OSN_eGFP+ and OSN_eGFP- indicating
200 that both OSNs are involved in synaptic transmission (Figures 5a and b).
201
202 We did not find major differences in transcriptome profiling between males and females for
203 genes that were differentially expressed between the three cell groups (Figure 5 – figure
204 supplement 3,4). We found a substantial number of olfactory receptor genes that were
205 differentially expressed between males and females (Figure 5 – figure supplement 4).
206 Surprisingly, the differentially expressed olfactory receptors differed from receptors identified by
207 van der Linden et al. (van der Linden et al., 2018). Finally, we compared expression of
208 transcripts involved in taste transduction, canonical olfactory transduction, and non-canonical

209 OSNs (Figure 4d). The non-canonical OSNs considered here included guanilyl-cyclase D (GC-
210 D) OSNs (Juilfs et al., 1997), Trpc2 OSNs (Omura and Mombaerts, 2014) and Cav2.1 OSNs
211 (Pyrski et al., 2018). Both OSN_eGFP+ and OSN_eGFP- expressed low levels of *Cancna1a*
212 encoding for Cav2.1 and *Trpc2*. OSN_eGFP- expressed higher levels of Trace amine-associated
213 receptors (Liberles, 2015) than OSN_eGFP+ cells. Both OSN_eGFP+ and OSN_eGFP-
214 expressed transcripts for OMP, BBS1 and 2 and proteins involved in the canonical olfactory
215 transduction pathway, markers of canonical OSNs.
216
217 **Gene ontology enrichment analysis reveals differences in chemosensory transduction and**
218 **synaptic vesicle function between the three groups of cells.** Perusal of the top differences
219 between the three cell groups suggested that these are distinct chemosensory cell types found in
220 the olfactory epithelium. Both OSN_eGFP+ and OSN_eGFP- share expression of OSN-specific
221 transcripts, express distinct subsets of olfactory receptors and differ in expression of the activity-
222 dependent transcript *S100a5*, and MVC_eGFP cells differ from both OSN groups in expression
223 of transcripts for synaptic transmission and for markers of mature OSNs and microvillous cells.
224 In order to perform a thorough analysis of the differences between these chemosensory cell
225 groups we performed an analysis of gene ontology (GO) enrichment for lists of genes related to
226 chemosensory perception. When compared with either OSN_eGFP+ or OSN_eGFP- we found
227 that MVC_eGFP cells were enriched for transcripts for the gene ontology list of sensory
228 perception of sweet/umami taste (GO:0050916 and GO:0050916) (Figure 5d, Figure 5 – figure
229 supplements 3,4) involving taste detection/transduction proteins that have been reported to be
230 expressed in MVCs (Genovese and Tizzano, 2018; Hegg et al., 2010): *Gnat3*, encoding for
231 gustducin, the G protein mediating sweet and umami taste transduction (McLaughlin et al.,

232 1992), *Itpr3*, encoding for the inositol-1,4,5-triphosphate receptor type 3 and *Tas1r3*, encoding
233 for a gustducin-coupled receptor involved in umami and sweet taste (Damak et al., 2003; Zhang
234 et al., 2003). Interestingly, the GO lists for sensory perception of sweet/umami taste
235 (GO:0050916 and GO:0050917) and other lists for sensory and taste perception (GO:0050906,
236 GO:0050912) are enriched in OSN_eGFP+ cells compared to OSN_eGFP- cells (Figure 4e,
237 Figure 4 – figure supplement 3, including *Gnat3, Itpr3, Tas1r3*). Furthermore, gene ontology
238 analysis for OSN_eGFP+ cells compared to OSN_eGFP- cells finds decreased enrichment for
239 sensory perception of smell (GO:0007608) and G protein-coupled receptor signaling pathways
240 (GO:0007186) that include a large number of olfactory receptors and transcripts encoding for
241 proteins involved in peripheral olfaction such as *Gfy*, *Omp*, *Pde1c* and *Pde4a* (GO:0007608) and
242 *Dgkg*, *Gng13*, *Itgb1*, *Nsg1* (GO:0007186). Finally, enrichment of gene ontology lists for synaptic
243 vesicle function were decreased for MVC_eGFP cells compared with either OSN_eGFP+ or
244 OSN_eGFP- cells (Figure 5c,d). Results of this gene ontology analysis of chemosensation and
245 synaptic vesicle function reinforces the finding that the three cell groups in this study are distinct
246 chemosensory cell types of the olfactory epithelium. OSN_eGFP+ cells are related to
247 MVC_eGFP cells because of expression of taste perception gene ontology, but differ from
248 MVC_eGFP cells in expression of olfactory receptors and transcripts related to synaptic function
249 as expected for an OSN.
250
251 **Gene ontology analysis finds enrichment of lists of viral-related, inflammation and immune**
252 **transcripts in MVC_eGFP cells and OSN_eGFP+ cells.** SCCs, tuft and brush cells have been
253 implicated in responses to bacterial and viral infection, immunity and inflammation (Luo et al.,
254 2019; Maina et al., 2018; O'Leary et al., 2019; Perniss et al., 2020; Rane et al., 2019; Saunders et

255 al., 2014; Tizzano et al., 2010; Ualiyeva et al., 2020). The fact that MVCs are closely related to
256 these cells (Fu et al., 2018; Genovese and Tizzano, 2018; Ogura et al., 2011) lead us to search for
257 gene ontology enrichment related to bacterial and viral infection, immunity and inflammation for
258 MVC_eGFP cells. We found robust enrichment of these gene ontologies in MVC_eGFP cells
259 and OSN_eGFP+ cells (Figures 4e, 5c,d). Transcripts related to viral infection that were higher
260 in MVC_eGFP cells and OSN_eGFP+ cells compared to OSN_eGFP- cells (Figure 6) including
261 those involved in viral entry into host cells, viral transcription and regulation of viral
262 transcription, negative regulation of viral genome replication and negative regulation of viral
263 process (Figures 4e, 5c, Figure 6 – figure supplements 1-3). We also found gene ontology
264 enrichment in MVC_eGFP cells and OSN_eGFP+ cells compared to OSN_eGFP- cells for
265 defense response to bacterium (Figure 6 – figure supplements 1-3).
266
267 Importantly, we also find enrichment for transcript expression for immunity and inflammation
268 (Figures 4e, 5c,d and Figure 6 – figure supplements 1-3). Genes related to inflammation and
269 immunity that were higher in MVC_eGFP cells and OSN_eGFP+ cells compared to
270 OSN_eGFP- cells are shown in Figure 6 – figure supplements 4-7. Among these transcripts *IL25*
271 and its receptor *Il17rb* are enriched in both MVC_eGFP cells and OSN_eGFP+ cells. In SCCs,
272 brush cells and tuft cell generation of IL25 leads to a type 2 inflammation and stimulates
273 chemosensory cell expansion in a sequence of events that also involves cysteinyl leukotrienes
274 (Bankova et al., 2018; Luo et al., 2019; von Moltke et al., 2016). The presence of both *Il25* and
275 *Il17rb* suggests an autocrine effect. Furthermore, both cell types displayed increased expression
276 of transcripts encoding for enzymes involved in eicosanoid biosynthesis such as *Alox5*, *Ptgs1*

277 and *Ptgs2* that are found in brush cells in the airways (Bankova et al., 2018) and tuft cells in the

278 intestine (McGinty et al., 2020) where they drive type 2 immune responses.

279

Discussion

We performed transcriptional profiling of three chemosensory cells in the mouse olfactory epithelium: MVC_eGFP cells and two types of OSNs: OSN_eGFP+ and OSN_eGFP-. We found that while the transcriptome of each of these cell types is distinct they share common features across groups. The two groups of OSNs share transcript expression for proteins expressed in OSNs such as OMP, olfactory transduction proteins, and proteins involved in synaptic function. Yet, they differ in olfactory receptor expression and OSN_eGFP+ express taste transduction transcripts and other transcripts found in SCCs such as *Il25* and *Pou2f3*. On the other hand, MVC_eGFP cells express transcripts encoding for taste transduction proteins and other transcripts found in SCCs such as *Pou2f3* but they do not express transcripts for proteins involved in olfactory transduction and synaptic function, and they do not express olfactory receptors. Finally, we found that MVC_eGFP cells and OSN_eGFP+ cells express a substantial number of transcripts involved in viral infection, inflammation and immunity.

Here we find that OSN_eGFP+ are OSNs expressing full-length TRPM5 in the adult mouse (Figure 3). This raises the question why our results differ from Pyrski and co-workers who did not find full-length TRPM5 in OSNs (Pyrski et al., 2017). Likely, this is due to differences in environmental conditions that alter the number of OSNs expressing TRPM5 in the adult mouse (Figure 2). Interestingly, consistent with our finding of TRPM5 expression in OSNs, analysis of scRNA data in the literature indicates that there are 8 OSNs expressing TRPM5 among 3209 OSNs in the data set from Ziegler and co-workers (Ziegler et al., 2020) and 3 OSNs expressing TRPM5 among 2113 OSNs in the data set from Wu and co-workers (Wu et al., 2018). Finally, OSN_eGFP+ express low levels of the activity-dependent transcript s100a5 (Fischl et al., 2014)

304 (Figure 4a) suggesting that these cells express olfactory receptors that are not stimulated by
305 odorants present in the cage.
306
307 Gene ontology analysis revealed that MVC_eGFP cells (and OSN_eGFP+ cells to a lesser
308 extent) are enriched in viral-related transcripts compared to OSN_eGFP- (Figures 4e, 5c,d, and
309 Figure 6 – figure supplements 1-3). To infect cells, viruses must interact with host cell
310 membranes to trigger membrane fusion and viral entry. Membrane proteins at the surface of the
311 host cell are thus key elements promoting or preventing viral infection. Here we find that
312 transcripts for several membrane proteins and cell adhesion molecules involved in viral entry are
313 enriched in MVC_eGFP cells. *Plscr1* encodes a phospholipid scramblase which has been shown
314 to promote herpes simplex virus (HSV) entry in human cervical or vaginal epithelial cells and
315 keratinocytes (Cheshenko et al., 2018), and hepatitis C virus entry into hepatocytes (Gong et al.,
316 2011). In contrast with its role in viral entry, PLSCR1 impairs the replication of other types of
317 viruses in infected cells (influenza A virus (Luo et al., 2018), hepatitis B virus (Yang et al.,
318 2012)). IFTM2 is another transmembrane protein that mediates viral entry. In contrast with
319 PLSCR1, IFTM2 inhibits viral entry of human immunodeficiency virus (HIV, (Yu et al., 2015)),
320 hepatitis C virus (Narayana et al., 2015), influenza A H1N1 virus, West Nile virus, and dengue
321 virus (Brass et al., 2009). IFTM2 also inhibits viral replication (Brass et al., 2009) and protein
322 synthesis (Lee et al., 2018). Nectins are transmembrane glycoproteins and constitute cell surface
323 receptors for numerous viruses. There is wide evidence that HSV can enter host cells through
324 Nectin-1 dependent mechanisms, particularly for neuronal entry (Kopp et al., 2009; Petermann et
325 al., 2015; Sayers and Elliott, 2016; Shukla et al., 2012), and Nectin-4 appears essential for
326 measles virus epithelial entry (Noyce and Richardson, 2012; Singh et al., 2015; Singh et al.,

327 2016). In addition to cell surface molecules, the mucus contains secreted proteins that confer
328 protection against viruses to the underlying cells. Glycoproteins are major constituents of mucus
329 and exhibit multiple pathogens binding-sites. We found the *Ltf* transcript in MVC_eGFP cells,
330 which encodes for lactotransferrin. Lactotransferrin is a globular glycoprotein widely represented
331 in the nasal mucus with anti-viral activity against Epstein-Barr virus (Zheng et al., 2014; Zheng
332 et al., 2012), HSV (Shestakov et al., 2012; Valimaa et al., 2009)) and Hepatitis C virus (Allaire et
333 al., 2015).
334
335 Viruses have developed numerous strategies to overcome barrier mechanisms to enter the cells.
336 After viral entry infected cells have other resources to fight against viral infection by disrupting
337 the production of new viral particles, limiting inflammation processes and activating innate
338 immune responses. For example, TRIM25 is an ubiquitin ligase that activates retinoic acid-
339 inducible gene I (RIG-I) to promote the antiviral interferon response (Gack et al., 2007).
340 Furthermore, influenza A virus targets TRIM25 to evade recognition by the host cell (Gack et al.,
341 2009). In addition, TRIM25 displays a nuclear role in restricting influenza A virus replication
342 (Meyerson et al., 2017). Zc3h12a, also known as MCPIP-1, inhibits hepatitis B and C virus
343 replication, reduces virus-induced inflammation (Li et al., 2020; Lin et al., 2014), and exerts
344 antiviral effects against influenza A virus (Dong et al., 2017). Finally, *Pou2f3* also called *Skn1a*,
345 encodes for a key regulator for the generation of TRPM5-expressing cells in various epithelial
346 tissues (Yamashita et al., 2017). *Pou2f3* transcript was increased in MVC_eGFP cells (and to a
347 lesser extent in OSN_eGFP+) compared to OSN_eGFP-. *Skn1a/Pou2f3*-deficient mice lack
348 intestinal tuft cells and have defective mucosal type 2 responses to helminth infection in the
349 intestine (Gerbe et al., 2016). Finally, both OSN_eGFP+ and MVC_eGFP cells express Il25, an

350 interleukin that is involved in the inflammatory response of TRPM5-expressing epithelial cells in
351 the airway epithelium and the gut (O'Leary et al., 2019), and in the skin Il25 expression leads to
352 disruption of the epithelium and enhances HSV-1 and vaccinia virus replication (Kim et al.,
353 2013).
354
355 Our findings of expression of virally relevant transcripts in MVC_eGFP cells complement
356 published studies on the role of MVC-related SCCs in viral infection. In the trachea, viral-
357 associated formyl peptides activate SCCs to release acetylcholine and activate mucocilliary
358 clearance by ciliated cells (Perniss et al., 2020). This activation is mediated by the TRPM5
359 transduction pathway in the SCC and muscarinic acetylcholine receptors in the ciliated cell. In a
360 similar manner in the olfactory epithelium MVCs respond to ATP, which is involved in
361 activating mucociliary movement by releasing acetylcholine and activating adjacent
362 sustentacular cells through a muscarinic receptor (Fu et al., 2018). Therefore, viral infection
363 could result in activation of MVCs resulting in activation of mucociliary clearance by adjacent
364 sustentacular cells. In addition, in the anterior olfactory epithelium, where there is a higher
365 density of MVCs, mice exposed to mild odorous irritants exhibited a time-dependent increase in
366 apoptosis and a loss of mature OSNs without a significant increase in proliferation or
367 neurogenesis (Lemons et al., 2020). Therefore, activation of MVCs by viruses could lead to loss
368 of mature OSNs contributing to smell loss after viral infection. Interestingly, in the mouse distal
369 lung, where there is no expression of SCCs, there was de novo generation of SCCs after infection
370 with A/H1N1/PR/8 influenza virus (Rane et al., 2019) raising the question whether virus
371 exposure could alter MVC number in the olfactory epithelium. Finally, because we find high
372 expression of transcripts involved in Type 2 immune response in MVCs viral activation of these

373 cells could result in activation of cytokine-induced inflammation by long-term horizontal basal
374 cells that activate type 1 immune responses within the olfactory epithelium (Chen et al., 2019).
375
376 The olfactory epithelium provides direct viral access to the brain through the olfactory nerve.
377 Whether this olfactory path constitutes route of entry for viruses to the brain is a matter of
378 intense discussion, especially because some viruses are postulated to be involved in
379 encephalopathy and neurodegenerative disorders (Dando et al., 2014; Doty, 2008). Our findings
380 that these TRPM5-bearing OSN_eGFP+ cells are enriched in virally-related genes suggests that
381 these cells may be involved in or prevention of viral entry into the brain (and these two
382 alternatives are not exclusive since they may be different for different viruses). On the one hand,
383 we identified transcripts encoding for viral receptors in OSN_eGFP+ cells, suggesting that
384 viruses can enter these OSNs. If viral particles were to enter the OSNs they could reach the
385 olfactory bulb through anterograde transport along the olfactory nerve and from the olfactory
386 bulb, viruses can spread throughout the brain along the olfactory bulb-hippocampus route. On
387 the other hand, we found enrichment for transcripts encoding for proteins involved in limiting
388 viral infection and promoting immune and anti-inflammatory responses in OSNs_eGFP+ and
389 MVC_eGFP cells. In this case, viral spread to the brain would be prevented. Finally, the
390 olfactory epithelium is innervated by the trigeminal nerve, and substance P immunostaining is
391 closely associated with subsets of MVCs (Lin et al., 2008). This raises the question whether an
392 interaction between MVCs and trigeminal nerve fibers could participate in local inflammation as
393 found for SCCs (Saunders et al., 2014), and could modulate the entry of virus to the brain stem
394 through the trigeminal nerve. Future experiments are necessary to study the potential role of
395 MVC_eGFP cells and OSNs_eGFP+ in viral infection of the olfactory epithelium and the brain.

396

397 Recently, due to the current COVID-19 pandemic, researchers have focused their attention on
398 investigating SARS-CoV-2 mechanism of entry into cells. SARS-CoV-2 targets mainly cells of
399 the respiratory pathway where viral entry is mediated by ACE2 and TMPRSS2 (Hoffmann et al.,
400 2020). Because numerous patients reported loss of smell (Giacomelli et al., 2020; Parma et al.,
401 2020; Yan et al., 2020a; Yan et al., 2020b), researchers wondered about the mechanism for
402 SARS-CoV-2 infection of the olfactory epithelium. In our study, we found the *Tmprss2*
403 transcript was significantly increased in MVC_eGFP cells and OSN_eGFP+ compared to
404 OSN_eGFP- (Figure 6). We did not find *Ace2* enrichment in these cells, but this may be due to
405 inefficiency in finding with RNAseq low abundance transcripts like *Ace2* (Ziegler et al., 2020).
406 Transcriptional profiling of single cells in the olfactory epithelium from other laboratories found
407 expression of transcripts for both *Tmprss2* and *Ace2* in in sustentacular cells and stem cells, and
408 at lower levels in MVCs (Brann et al., 2020; Fodoulian et al., 2020). Viral infection of
409 sustentacular cells may explain loss of smell because these cells play a key role in supporting
410 olfactory function by providing glucose for the energy necessary for olfactory transduction in the
411 OSN cilia (Villar et al., 2017). Importantly, type I interferons, and to a lesser extent type II
412 interferons induced by response of the host to SARS-CoV-2, and infection by other viruses
413 inducing the interferon pathway increases *Ace2* expression in the nasal epithelium (Ziegler et al.,
414 2020). MVCs may play a role in SARS-CoV-2 infection of the olfactory epithelium because
415 these cells may participate in activating inflammation of the epithelium that elicits type 1
416 immune response (Chen et al., 2019). Finally, our finding of transcripts involved in viral entry,
417 replication and defense in a subset of OSNs raises the question whether viruses enter the central
418 nervous system through the olfactory nerve (Bilinska et al., 2020). This is relevant to the

potential long term effect of SARS-CoV-2 and other viruses in neurological and neurodegenerative disorders (De Felice et al., 2020). Our study provides new insights into a potential role for TRPM5-expressing cells in viral infection of the main olfactory epithelium.

422 **Materials and Methods**

423 **Key Resources Table**

REAGENT TYPE	REAGENT or RESOURCE	SOURCE	IDENTIFIER	ADDITIONAL INFORMATION
Chemical compound, drug	BrainPhys Neuronal Medium	Stemcell Technologies		Product # 05791
Chemical compound, drug	Dispase II	Sigma		Product # D4693
Chemical compound, drug	AcGFP1/eGFP calibration beads	Takara		Flow cytometry calibration beads Product # 632594
Chemical compound, drug	mCherry calibration beads	Takara		Flow cytometry calibration beads Product # 632595
Chemical compound, drug	RQ1 RNase-free DNase	Promega		Product # M6101
Chemical compound, drug	Papain	Sigma		Product # P3125
Chemical compound, drug	Paraformaldehyde (32%)	Electron Microscopy Sciences		Product # 157145
Chemical compound, drug	RNAprotect Tissue Reagent	Qiagen		Product # 76526
Chemical compound, drug	RNeasy Plus Micro Kit	Qiagen		Product # 74034
Chemical compound, drug	High Capacity c-DNA Reverse Transcription kit	ABI		
Chemical compound, drug	18s rRNA	PE ABI		
Strain, strain background	TRPM5-eGFP	Dr. Robert Margolskee (Clapp et al., 2006)		
Strain, strain background	OMP-H2B::Cherry	Generated for this publication		This mouse will be deposited in Jackson Laboratories
Software, algorithm	MATLAB_R2018a	Mathworks	RRID: SCR_001622	
Software, algorithm	Illustrator	Adobe	RRID: SCR_010279	
Software, algorithm	Photoshop	Adobe	RRID: SCR_014199	

Software, algorithm	InDesign	Adobe		
Software, algorithm	MoFlo Astrios Summit Software (6.3.1.16945).	Beckman Coulter		
Software, algorithm	BBMap (BBDuk)		RRID:SCR_016968	
Software, algorithm	Salmon v1.2.1	https://combine-lab.github.io/salmon/	RRID:SCR_017036	(Patro et al., 2017)
Software, algorithm	DeSEQ2 v1.28.0	bioconductor.org https://bioconductor.org/packages/release/bioc/html/DESeq2.html	RRID:SCR_015687	(Love et al., 2014)
Software, algorithm	TopGO, v2.40.0		RRID:SCR_014798	
Software, algorithm	pHeatmap, 1.0.12		RRID:SCR_016418	
Software, algorithm	Ensembl GRCm38, v99			
Software, algorithm	R, v4.0		RRID:SCR_001905	
Software, algorithm	Tximport, v1.16.0		RRID:SCR_016752	
Software, algorithm	SAMtools	SAMtools http://samtools.sourceforge.net/	RRID:SCR_002105	(Li et al., 2009)
Software, algorithm	Bedtools		RRID:SCR_006646	
Software, algorithm	STAR v2.5.3a	https://github.com/alexdobin/STAR	RRID:SCR_015899	
Software, algorithm	Sigmaplot, v12.5	Systat Software	RRID:SCR_003210	
Software, algorithm	Custom code for bioinformatics analysis	https://github.com/eric-d-larson/OE_TRPM5		

424

425 **Overview of the method for transcriptional profiling of low abundance cell populations.** For
426 transcriptional profiling of TRPM5-bearing MVC_eGFP cells and OSN_eGFP+ cells that
427 constitute a small fraction of the cells in the epithelium, we used FACS to separate the cell
428 populations targeted for RNAseq (Amamoto et al., 2019). In our experiments, we isolated the
429 cells from mice that expressed fluorescent marker proteins appropriate for cell sorting. OSNs
430 were expressing mCherry under the control of OMP promoter. eGFP was expressed in MVCs
431 and a subset of OSNs (OSN_eGFP+ cells) under control of the TRPM5 promoter.
432
433 **Generation of OMP-H2B::Cherry mice**. A PacI cassette containing PacI-H2B::mCherry-pA
434 PGK-puro-pA-PacI was inserted into an OMP gene-targeting vector (pPM9)(Mombaerts et
435 al., 1996), which replaces the OMP coding sequence with the PacI cassette and expresses a
436 H2B::mCherry fusion protein. Animals are maintained in a mixed 129/B6 background.
437
438 **Animals.** Mice with TRPM5-driven eGFP expression (Clapp et al.,2006) were crossed with
439 OMP-H2B::Cherry mice. Both lines were maintained separately as homozygous and
440 backcrossed regularly. Experiments were performed on mice from the F1 generation cross of
441 TRPM5-eGFP and OMP-H2B::Cherry mice (OMP-H2B::mCherry/TRPM5-eGFP). PCR was
442 used to verify genotype of experimental mice for eGFP and mCherry expression. Both male and
443 female mice were used for experiments with ages ranging from 3- 8 months. Estrous and cage
444 mate information was collected for all female mice in conjunction with experimental use. Mice
445 were housed in passive air exchange caging under a 12:12 light/dark cycle and were given food
446 and water *ad libitum*. Mice were housed in the National Institutes of Health approved Center for
447 Comparative Medicine at the University of Colorado Anschutz Medical Campus. All procedures

448 were performed in compliance with University of Colorado Anschutz Medical Campus
449 Institutional Animal Care and Use Committee (IACUC).
450
451 **Tissue dissociation of the olfactory epithelium.** Following euthanasia via CO2 inhalation, the
452 olfactory epithelium was immediately removed from the nasal cavity and epithelial tissue was
453 separated from the bone in the turbinates. Care was taken not to include respiratory epithelium.
454 The epithelium was dissociated enzymatically with Dispase II (2 mg/ml) diluted in Ringer's
455 solution (145mM NaCl, 5mM KCL, 20mM HEPES, 1mM $MgCL_2$, 1mM $CaCl_2$, 1mM Ny-
456 Pyruvate, 5mM Glucose) (~25 minutes at 37^0C) followed by an incubation in a papain plus
457 Ca/Mg++ free Ringer's solution (Ca/Mg++ free Ringer's: 145mM NaCl, 5mM KCL, 20mM
458 HEPES, 1mM Ny-Pyruvate, 1mM EDTA , L-cysteine: 1mg L-cysteine /1.5mL Ca/Mg++ free
459 Ringer's, Papain:1-3ul/1mL Ca/Mg++ free Ringer's), for ~40-45 minutes at 37^0C. Following
460 incubation, DNase I (Promega) at 0.05U/µl and RNAse free 10x Reaction buffer (1:20) were
461 added to solution and the tissue was gently triturated using a ~1mm opening pipette. Isolated
462 OSNs were collected from supernatants via centrifugation and resuspended in cell sorting
463 medium of 1x PBS (diluted from commercial 10x PBS, pH 7.4) and BrainPhys Neuronal
464 Medium (Stemcell Technologies). Initially, isolated cells were examined with a confocal
465 microscope to confirm efficacy of dissociation methods, and examine cell types and
466 fluorescence. For RNAseq, cells were strained through a 40 µm cell strainer and kept on ice until
467 sorted via flow cytometry.
468
469 **Flow cytometry.** Fluorescence activated cell sorting was performed in the University of
470 Colorado Cancer Center Flow Cytometry Core on a Beckman Coulter MoFlo Astrios EQ using

471 MoFlo Astrios Summit Software (6.3.1.16945). eGFP signal was detected using a 488 nm laser
472 and a bandpass 526/52nm collection filter. mCherry signal was detected using a 561 nm laser
473 and a bandpass 614/20 nm collection filter. The 488nm laser was also used to detect light
474 scatter. The threshold was set at 3%. Gating was set to exclude doublets and optimized as cell
475 populations emerged based on fluorescent markers. Flow cytometry calibration beads for
476 AcGFP1/eGFP and mCherry (Takara, 632594, 632595) were used as fluorescence intensity
477 controls. Olfactory epithelium cell suspensions from wild type and OMP-H2B::Cherry mice or
478 TRPM5-eGFP mice were sorted as controls for auto fluorescence for eGFP and mCherry
479 populations respectively. Cells were sorted into RNAprotect Tissue Reagent (Qiagen).
480
481 **RNA-extraction.** Total RNA was extracted from sorted, pooled cells from each cell population
482 using the RNeasy Plus Micro Kit (Qiagen) according to the manufacturers recommended
483 protocol.
484
485 **RT-qPCR.** Quantitative reverse transcription polymerase chain reaction (RT-qPCR) was used to
486 assess and confirm identities of cell types from each of the sorted cell populations. Following
487 total RNA extraction, RT-qPCR was performed in the PCR core at University of Colorado
488 Anschutz Medical Campus for the following markers: OMP, TRPM5, eGFP and ChAT. Primers
489 and probes used for eGFP, TRPM5 and OMP were described in (Oshimoto et al., 2013).
490 Predesigned primers and probes for ChAT were purchased from Life Technologies. The mRNA
491 for these targets was measured by RT-qPCR using ABI QuantStudio 7 flex Sequence detector.
492 1μg total RNA was used to synthesize cDNA using the High Capacity c-DNA Reverse
493 Transcription kit (ABI-P/N 4368814). cDNA was diluted 1: 2 before PCR amplification.

494

495 The TaqMan probes were 5'labeled with 6-carboxyfluorescein (FAM). Real time PCR reactions
496 were carried out in MicroAmp optical tubes (PE ABI) in a 25 µl mix containing 8 % glycerol,
497 1X TaqMan buffer A (500 mM KCl, 100 mM Tris-HCl, 0.1 M EDTA, 600 nM passive
498 reference dye ROX, pH 8.3 at room temperature), 300 µM each of dATP, dGTP, dCTP and 600
499 µM dUTP, 5.5 mM MgCl2, 1X primer-probe mix, 1.25 U AmpliTaq Gold DNA and 5 µl
500 template cDNA. Thermal cycling conditions were as follows: Initiation was performed at 50ºC
501 for 2 min followed by activation of TaqGold at 95ºC for 10 min. Subsequently 40 cycles of
502 amplification were performed at 95ºC for 15 secs and 60ºC for 1 min. Experiments were
503 performed with duplicates for each data point. Each PCR run included the standard curve (10
504 fold serially diluted pooled cDNA from control and experimental samples), test samples, no-
505 template and NORT controls. The standard curve was then used to calculate the relative
506 amounts of targets in test samples. Quantities of targets in test samples were normalized to the
507 corresponding 18s rRNA (PE ABI, P/N 4308310).

508

509 **RNA sequencing and pre-processing.** RNA quality control, library preparation, and sequencing
510 were performed at the University of Colorado Genomics and Microarray core. Extracted RNA
511 was used as the input for the Nugen Universal Plus mRNA-seq kit (Redwood City, CA) to build
512 stranded sequencing libraries. Indexed libraries were sequenced using an Illumina
513 NovaSEQ6000. Library preparation and sequencing was performed in two batches, separated by
514 gender. 11 female samples were sequenced with an average depth of 37.3 million +/- SD of 6.5
515 million read pairs, and 25 male samples were sequenced with an average depth of 34.8 million
516 +/- SD of 3.5 million read pairs. Metadata for the samples submitted are shown in Figure 4 –

517 figure supplement 2. Raw BCL files were demultiplexed and converted to FASTQ format.
518 Trimming, filtering, and adapter contamination removal was performed using BBDuk
519 (Bushnell).
520
521 **RNA Sequencing Analysis.** Transcript abundance was quantified from trimmed and filtered
522 FASTQ files using Salmon v1.2.1(Patro et al., 2017) and a customized Ensembl GRCm38
523 (release 99) transcriptome (Zerbino et al., 2018). A customized version of the transcriptome was
524 prepared by appending FASTA sequences of eGFP and mCherry to the GRCm38 FASTA file.
525 The corresponding gene transfer format (GTF) file was modified accordingly to incorporate the
526 new transcripts. Transcript abundance was summarized at the gene level using the TxImport
527 (Soneson et al., 2015) package in R. Differential gene expression was quantified using DESeq2
528 (Love et al., 2014) with default parameters after removing genes with an average count of < 5
529 reads in each group. Significance was determined by FDR-adjusted p-value < 0.05. TopGO was
530 used for gene ontology analysis (Alexa and Rahnenfuhrer, 2020). The input to TopGO was a list
531 of significant DEGs and a list of all detected genes in the dataset. Enrichment was calculated by
532 dividing the number of detected genes by the number of expected genes within each ontology of
533 the TopGO output. To make the bar graphs in Figures 4 and 5, enrichment scores of
534 downregulated GO terms were multiplied by -1 for visualization. Heatmap visualization was
535 performed using *pHeatmap* in R (Kolde, 2019).
536
537 **TRPM5 exon coverage.** To visualize exon coverage of *Trpm5*, trimmed and filtered FASTQ
538 files were mapped to the Ensembl GRCm38 (version 99) using STAR (params, version
539 2.5.3a)(Dobin et al., 2013). The genome FASTA and GTF files were modified as described

540 above. Read coverage was summarized by *Trpm5* exon using a combination of Samtools ('depth'
541 and 'bedcov')(Li et al., 2009) and Bedtools (Quinlan and Hall, 2010). Data were compared using
542 a Scheirer-Ray-Hare test in R (*rcompanion* package).
543
544 **Tissue Preparation for Fluorescence Microscopy and *in situ*.** For euthanasia, mice were
545 anesthetized with ketamine/xylazine (20–100 _g/g of body weight), perfused transcardially with
546 0.1 M phosphate buffer (PBS) followed by a PBS-buffered fixative (EMS 32%
547 Paraformaldehyde aqueous solution diluted to 4% with 1x PBS) . The nose was harvested and
548 postfixed for 12 h before being transferred for cryoprotection into PBS with 20% sucrose
549 overnight. The olfactory epithelium was cryosectioned coronally into 16 μm -thick sections
550 mounted on Superfrost Plus slides (VWR, West Chester, PA).
551
552 ***In situ.*** *In situ* hybridization was performed with the hybridization chain reaction method (Choi
553 et al., 2018) using HCR v3.0 Probe Sets, Amplifiers, and Buffers from Molecular Instruments,
554 Inc. Frozen slides were allowed to thaw and dry, then immersed in 70% ethanol overnight at
555 4°C, and allowed to dry again completely. Slides were inverted and placed on a Plexiglas
556 platform inside a humidified chamber; subsequent steps were performed using this setup. Slides
557 were incubated in 10 μg/μl proteinase K for 10 minutes at 37°C, then pre-hybridized with HCR
558 hybridization buffer (30% formamide buffer from Molecular Instruments) for 10 minutes at
559 37°C. *Trpm5-B3* probes and *OMP-B2* probes (0.4 pmol of each probe in 100 μl HCR
560 hybridization buffer per slide) were added, and slides were hybridized overnight at 37°C. Slides
561 were briefly incubated in undiluted HCR Wash Buffer (30% formamide buffer from Molecular
562 Instruments) at 37°C. Excess probes were removed by incubating slides for 15 minutes each at

563 37°C in solutions of 75% HCR Wash Buffer / 25% SSCT (5X SSC, 0.1% Tween, diluted in
564 RNAse free water), 50% Buffer / 50% SSCT, 25% Buffer / 75% SSCT, and 100% SSCT. Slides
565 were incubated in Amplification Buffer (Molecular Instruments) at room temperature for 30
566 minutes. B3 hairpins labeled with Alexa Fluor 647 and B2 hairpins labeled with Alexa Fluor 546
567 were prepared (6 pmol of each hairpin were heat shocked, then cooled for 30 minutes, and added
568 to 100µl of Amplification Buffer) added to slides, and incubated overnight at room temperature.
569 Excess hairpins were removed with three washes in SSCT at room temperature. Tissue was
570 counterstained with DAPI, and slides were mounted using Invitrogen SlowFade Diamond
571 Antifade Mountant (Thermo Fisher Scientific).
572
573 **Fluorescence microscopy.** Microscopy was performed with confocal microscopes (Nikon A1R
574 or 3i Marianas). Images shown are flattened Z stacks. In situ images in Figure 3 were
575 deconvolved in DeconvolutionLab 2 (Sage et al., 2017) using 10 rounds of Lucy-Richardson
576 deconvolution (Lucy, 1974; Richardson, 1972) and a theoretical point spread function (PSF).
577 The theoretical PSF was calculated using the Gibson-Lanni model (Gibson and Lanni, 1989) for
578 325 nm lateral and 800 nm axial pixel size, wavelength of the reporter dye molecule, and an air-
579 immersion 20X NA 0.75 objective. Image was maximum projected and Gamma of 0.8 applied to
580 the TRMP5 channel for viewing.
581
582 **Statistical analysis.** Statistical analysis was performed in Matlab (Mathworks, USA). Statistical
583 significance was estimated using a generalized linear model (GLM), with post-hoc tests for all
584 data pairs corrected for multiple comparisons using false discovery rate (Curran-Everett, 2000).
585 The post hoc comparisons between pairs of data were performed either with a t-test, or a ranksum

586 test, depending on the result of an Anderson-Darling test of normality. 95% CIs shown in the
587 figures as vertical black lines or shading bounding the lines were estimated by bootstrap analysis
588 of the mean by sampling with replacement 1000 times using the bootci function in MATLAB.
589
590
591 **Data availability.** All data will be available in NCBI GEO. The code used for bioinformatics
592 analysis is found in https://github.com/eric-d-larson/OE_TRPM5
593
594

595 ***Acknowledgements:*** We would like to acknowledge the support of Nicole Arevalo for laboratory
596 support, Jerome Artus and Anna-Katerina Hadjantonakis for the construction of the targeting
597 vector and production of OMP-H2B::Cherry mice. This work was supported by NIDCD
598 DC014253 (DR) and by the RNA Bioscience Initiative of the University of Colorado Anschutz
599 Medical Campus (DS and DR). A Starr Stem Cell Grant (JA, AKH and PF) supported the
600 production and characterization of the OMP-H2B::mCherry mouse strain.
601
602 ***Declaration of interests:*** The authors declare no competing interests.
603

604 Alexa, A., and Rahnenfuhrer, J. (2020). topGO: Enrichment Analysis for Gene Ontology (R
605 Package).

606 Allaire, A., Picard-Jean, F., and Bisaillon, M. (2015). Immunofluorescence to Monitor the
607 Cellular Uptake of Human Lactoferrin and its Associated Antiviral Activity Against the Hepatitis
608 C Virus. J Vis Exp.

609 Amamoto, R., Garcia, M.D., West, E.R., Choi, J., Lapan, S.W., Lane, E.A., Perrimon, N., and
610 Cepko, C.L. (2019). Probe-Seq enables transcriptional profiling of specific cell types from
611 heterogeneous tissue by RNA-based isolation. Elife *8*.

612 Bankova, L.G., Dwyer, D.F., Yoshimoto, E., Ualiyeva, S., McGinty, J.W., Raff, H., von Moltke,
613 J., Kanaoka, Y., Frank Austen, K., and Barrett, N.A. (2018). The cysteinyl leukotriene 3 receptor
614 regulates expansion of IL-25-producing airway brush cells leading to type 2 inflammation. Sci
615 Immunol *3*.

616 Bilinska, K., Jakubowska, P., Von Bartheld, C.S., and Butowt, R. (2020). Expression of the
617 SARS-CoV-2 Entry Proteins, ACE2 and TMPRSS2, in Cells of the Olfactory Epithelium:
618 Identification of Cell Types and Trends with Age. ACS Chemical Neuroscience.

619 Brann, D.H., Tsukahara, T., Weinreb, C., Lipovsek, M., Van den Berge, K., Gong, B., Chance,
620 R., Macaulay, I.C., Chou, H.-j., Fletcher, R.*, et al.* (2020). Non-neuronal expression of SARS-
621 CoV-2 entry genes in the olfactory system suggests mechanisms underlying COVID-19-
622 associated anosmia. bioRxiv, 2020.2003.2025.009084.

623 Brass, A.L., Huang, I.C., Benita, Y., John, S.P., Krishnan, M.N., Feeley, E.M., Ryan, B.J.,
624 Weyer, J.L., van der Weyden, L., Fikrig, E.*, et al.* (2009). The IFITM proteins mediate cellular
625 resistance to influenza A H1N1 virus, West Nile virus, and dengue virus. Cell *139*, 1243-1254.

626 Bushnell, B. BBMap (SourceForge).

627 Chen, M., Reed, R.R., and Lane, A.P. (2019). Chronic Inflammation Directs an Olfactory Stem
628 Cell Functional Switch from Neuroregeneration to Immune Defense. Cell Stem Cell *25*, 501-513
629 e505.

630 Cheshenko, N., Pierce, C., and Herold, B.C. (2018). Herpes simplex viruses activate
631 phospholipid scramblase to redistribute phosphatidylserines and Akt to the outer leaflet of the
632 plasma membrane and promote viral entry. PLoS Pathog *14*, e1006766.

633 Choi, H.M., Schwarzkopf, M., Fornace, M.E., Acharya, A., Artavanis, G., Stegmaier, J., Cunha,
634 A., and Pierce, N.A. (2018). Third-generation in situ hybridization chain reaction: multiplexed,
635 quantitative, sensitive, versatile, robust. Development *145*, dev165753.

636 Chuang, Y.C., Lee, C.H., Sun, W.H., and Chen, C.C. (2018). Involvement of advillin in
637 somatosensory neuron subtype-specific axon regeneration and neuropathic pain. Proc Natl Acad
638 Sci U S A *115*, E8557-E8566.

639 Clapp, T.R., Medler, K.F., Damak, S., Margolskee, R.F., and Kinnamon, S.C. (2006). Mouse
640 taste cells with G protein-coupled taste receptors lack voltage-gated calcium channels and
641 SNAP-25. BMC Biol *4*, 7.

642 Curran-Everett, D. (2000). Multiple comparisons: philosophies and illustrations. AmJPhysiol
643 RegulIntegrComp Physiol *279*, R1-R8.

644 Damak, S., Rong, M., Yasumatsu, K., Kokrashvili, Z., Varadarajan, V., Zou, S., Jiang, P.,
645 Ninomiya, Y., and Margolskee, R.F. (2003). Detection of sweet and umami taste in the absence
646 of taste receptor T1r3. Science *301*, 850-853.

647 Dando, S.J., Mackay-Sim, A., Norton, R., Currie, B.J., St John, J.A., Ekberg, J.A.K., Batzloff,
648 M., Ulett, G.C., and Beacham, I.R. (2014). Pathogens Penetrating the Central Nervous System:
649 Infection Pathways and the Cellular and Molecular Mechanisms of Invasion. Clinical
650 Microbiology Reviews *27*, 691-726.

651 De Felice, F.G., Tovar-Moll, F., Moll, J., Munoz, D.P., and Ferreira, S.T. (2020). Severe Acute
652 Respiratory Syndrome Coronavirus 2 (SARS-CoV-2) and the Central Nervous System. Trends in
653 Neurosciences.

654 Dobin, A., Davis, C.A., Schlesinger, F., Drenkow, J., Zaleski, C., Jha, S., Batut, P., Chaisson,
655 M., and Gingeras, T.R. (2013). STAR: ultrafast universal RNA-seq aligner. Bioinformatics *29*,
656 15-21.

657 Dong, C., Sun, X., Guan, Z., Zhang, M., and Duan, M. (2017). Modulation of influenza A virus
658 replication by microRNA-9 through targeting MCPIP1. J Med Virol *89*, 41-48.

659 Doty, R.L. (2008). The olfactory vector hypothesis of neurodegenerative disease: is it viable?
660 Ann Neurol *63*, 7-15.

661 Farbman, A.I., and Margolis, F.L. (1980). Olfactory marker protein during ontogeny:
662 immunohistochemical localization. Developmental biology *74*, 205-215.

663 Fischl, A.M., Heron, P.M., Stromberg, A.J., and McClintock, T.S. (2014). Activity-dependent
664 genes in mouse olfactory sensory neurons. Chem Senses *39*, 439-449.

665 Fodoulian, L., Tuberosa, J., Rossier, D., Landis, B.N., Carleton, A., and Rodriguez, I. (2020).
666 SARS-CoV-2 receptor and entry genes are expressed by sustentacular cells in the human
667 olfactory neuroepithelium. bioRxiv, 2020.2003.2031.013268.

668 Fu, Z., Ogura, T., Luo, W., and Lin, W. (2018). ATP and Odor Mixture Activate TRPM5-
669 Expressing Microvillous Cells and Potentially Induce Acetylcholine Release to Enhance
670 Supporting Cell Endocytosis in Mouse Main Olfactory Epithelium. Front Cell Neurosci *12*, 71.

671 Gack, M.U., Albrecht, R.A., Urano, T., Inn, K.S., Huang, I.C., Carnero, E., Farzan, M., Inoue,
672 S., Jung, J.U., and Garcia-Sastre, A. (2009). Influenza A virus NS1 targets the ubiquitin ligase
673 TRIM25 to evade recognition by the host viral RNA sensor RIG-I. Cell Host Microbe *5*, 439-
674 449.

675 Gack, M.U., Shin, Y.C., Joo, C.H., Urano, T., Liang, C., Sun, L., Takeuchi, O., Akira, S., Chen,
676 Z., Inoue, S., *et al.* (2007). TRIM25 RING-finger E3 ubiquitin ligase is essential for RIG-I-
677 mediated antiviral activity. Nature *446*, 916-920.

678 Genovese, F., and Tizzano, M. (2018). Microvillous cells in the olfactory epithelium express
679 elements of the solitary chemosensory cell transduction signaling cascade. PLoS One *13*,
680 e0202754.

681 Gerbe, F., Sidot, E., Smyth, D.J., Ohmoto, M., Matsumoto, I., Dardalhon, V., Cesses, P.,
682 Garnier, L., Pouzolles, M., Brulin, B., *et al.* (2016). Intestinal epithelial tuft cells initiate type 2
683 mucosal immunity to helminth parasites. Nature *529*, 226-230.

684 Giacomelli, A., Pezzati, L., Conti, F., Bernacchia, D., Siano, M., Oreni, L., Rusconi, S.,
685 Gervasoni, C., Ridolfo, A.L., Rizzardini, G., *et al.* (2020). Self-reported olfactory and taste
686 disorders in SARS-CoV-2 patients: a cross-sectional study. Clin Infect Dis.

687 Gibson, S.F., and Lanni, F. (1989). Diffraction by a circular aperture as a model for three-
688 dimensional optical microscopy. J Opt Soc Am A *6*, 1357-1367.

689 Gong, Q., Cheng, M., Chen, H., Liu, X., Si, Y., Yang, Y., Yuan, Y., Jin, C., Yang, W., He, F., *et*
690 *al.* (2011). Phospholipid scramblase 1 mediates hepatitis C virus entry into host cells. FEBS Lett
691 *585*, 2647-2652.

692 Hegg, C.C., Jia, C., Chick, W.S., Restrepo, D., and Hansen, A. (2010). Microvillous cells
693 expressing IP3 receptor type 3 in the olfactory epithelium of mice. Eur J Neurosci *32*, 1632-
694 1645.

695 Hoffmann, M., Kleine-Weber, H., Schroeder, S., Kruger, N., Herrler, T., Erichsen, S.,
696 Schiergens, T.S., Herrler, G., Wu, N.H., Nitsche, A.*, et al.* (2020). SARS-CoV-2 Cell Entry
697 Depends on ACE2 and TMPRSS2 and Is Blocked by a Clinically Proven Protease Inhibitor. Cell
698 *181*, 271-280 e278.

699 Jablonka-Shariff, A., Lu, C.Y., Campbell, K., Monk, K.R., and Snyder-Warwick, A.K. (2020).
700 Gpr126/Adgrg6 contributes to the terminal Schwann cell response at the neuromuscular junction
701 following peripheral nerve injury. Glia *68*, 1182-1200.

702 Juilfs, D.M., Fulle, H.J., Zhao, A.Z., Houslay, M.D., Garbers, D.L., and Beavo, J.A. (1997). A
703 subset of olfactory neurons that selectively express cGMP-stimulated phosphodiesterase (PDE2)
704 and guanylyl cyclase-D define a unique olfactory signal transduction pathway. Proc Natl Acad
705 Sci U S A *94*, 3388-3395.

706 Kim, B.E., Bin, L., Ye, Y.M., Ramamoorthy, P., and Leung, D.Y.M. (2013). IL-25 enhances
707 HSV-1 replication by inhibiting filaggrin expression, and acts synergistically with Th2 cytokines
708 to enhance HSV-1 replication. J Invest Dermatol *133*, 2678-2685.

709 Kolde, R. (2019). pheatmap: Pretty Heatmaps (cran.r-project.org).

710 Kopp, S.J., Banisadr, G., Glajch, K., Maurer, U.E., Grunewald, K., Miller, R.J., Osten, P., and
711 Spear, P.G. (2009). Infection of neurons and encephalitis after intracranial inoculation of herpes
712 simplex virus requires the entry receptor nectin-1. Proc Natl Acad Sci U S A *106*, 17916-17920.

713 Lee, W.J., Fu, R.M., Liang, C., and Sloan, R.D. (2018). IFITM proteins inhibit HIV-1 protein
714 synthesis. Sci Rep *8*, 14551.

715 Lemons, K., Fu, Z., Aoude, I., Ogura, T., Sun, J., Chang, J., Mbonu, K., Matsumoto, I.,
716 Arakawa, H., and Lin, W. (2017). Lack of TRPM5-Expressing Microvillous Cells in Mouse
717 Main Olfactory Epithelium Leads to Impaired Odor-Evoked Responses and Olfactory-Guided
718 Behavior in a Challenging Chemical Environment. eNeuro *4*.

719 Lemons, K., Fu, Z., Ogura, T., and Lin, W. (2020). TRPM5-expressing Microvillous Cells
720 Regulate Region-specific Cell Proliferation and Apoptosis During Chemical Exposure.
721 Neuroscience *434*, 171-190.

722 Li, H., Handsaker, B., Wysoker, A., Fennell, T., Ruan, J., Homer, N., Marth, G., Abecasis, G.,
723 Durbin, R., and Genome Project Data Processing, S. (2009). The Sequence Alignment/Map
724 format and SAMtools. Bioinformatics *25*, 2078-2079.

725 Li, M., Yang, J., Zhao, Y., Song, Y., Yin, S., Guo, J., Zhang, H., Wang, K., Wei, L., Li, S*., et al.*
726 (2020). MCPIP1 inhibits Hepatitis B virus replication by destabilizing viral RNA and negatively
727 regulates the virus-induced innate inflammatory responses. Antiviral Res *174*, 104705.

728 Liberles, S.D. (2015). Trace amine-associated receptors: ligands, neural circuits, and behaviors.
729 Current opinion in neurobiology *34*, 1-7.

730 Lin, R.J., Chu, J.S., Chien, H.L., Tseng, C.H., Ko, P.C., Mei, Y.Y., Tang, W.C., Kao, Y.T.,
731 Cheng, H.Y., Liang, Y.C.*, et al.* (2014). MCPIP1 suppresses hepatitis C virus replication and
732 negatively regulates virus-induced proinflammatory cytokine responses. J Immunol *193*, 4159-
733 4168.

734 Lin, W., Ezekwe, E.A., Jr., Zhao, Z., Liman, E.R., and Restrepo, D. (2008). TRPM5-expressing
735 microvillous cells in the main olfactory epithelium. BMC Neurosci *9*, 114.

736 Lin, W., Margolskee, R., Donnert, G., Hell, S.W., and Restrepo, D. (2007). Olfactory neurons
737 expressing transient receptor potential channel M5 (TRPM5) are involved in sensing
738 semiochemicals. Proc Natl Acad Sci U S A *104*, 2471-2476.

739 Lopez, F., Delgado, R., Lopez, R., Bacigalupo, J., and Restrepo, D. (2014). Transduction for
740 Pheromones in the Main Olfactory Epithelium Is Mediated by the Ca2+-Activated Channel
741 TRPM5. J Neurosci *34*, 3268-3278.

742 Love, M.I., Huber, W., and Anders, S. (2014). Moderated estimation of fold change and
743 dispersion for RNA-seq data with DESeq2. Genome Biol *15*, 550.

744 Lucy, L.B. (1974). An iterative technique for the rectification of observed distributions. The
745 Astronomical Journal *79*, 745.

746 Luo, W., Zhang, J., Liang, L., Wang, G., Li, Q., Zhu, P., Zhou, Y., Li, J., Zhao, Y., Sun, N., *et al.*
747 (2018). Phospholipid scramblase 1 interacts with influenza A virus NP, impairing its nuclear
748 import and thereby suppressing virus replication. PLoS Pathog *14*, e1006851.

749 Luo, X.C., Chen, Z.H., Xue, J.B., Zhao, D.X., Lu, C., Li, Y.H., Li, S.M., Du, Y.W., Liu, Q.,
750 Wang, P., *et al.* (2019). Infection by the parasitic helminth Trichinella spiralis activates a Tas2r-
751 mediated signaling pathway in intestinal tuft cells. Proc Natl Acad Sci U S A *116*, 5564-5569.

752 Maina, I.W., Workman, A.D., and Cohen, N.A. (2018). The role of bitter and sweet taste
753 receptors in upper airway innate immunity: Recent advances and future directions. World J
754 Otorhinolaryngol Head Neck Surg *4*, 200-208.

755 McGinty, J.W., Ting, H.-A., Billipp, T.E., Nadjsombati, M.S., Khan, D.M., Barrett, N.A., Liang,
756 H.-E., Matsumoto, I., and von Moltke, J. (2020). Tuft-Cell-Derived Leukotrienes Drive Rapid
757 Anti-helminth Immunity in the Small Intestine but Are Dispensable for Anti-protist Immunity.
758 Immunity *52*, 528-541.e527.

759 McLaughlin, S.K., McKinnon, P.J., and Margolskee, R.F. (1992). Gustducin is a taste-cell-
760 specific G protein closely related to the transducins. Nature *357*, 563-569.

761 Meyerson, N.R., Zhou, L., Guo, Y.R., Zhao, C., Tao, Y.J., Krug, R.M., and Sawyer, S.L. (2017).
762 Nuclear TRIM25 Specifically Targets Influenza Virus Ribonucleoproteins to Block the Onset of
763 RNA Chain Elongation. Cell Host Microbe *22*, 627-638 e627.

764 Mobley, A.S., Miller, A.M., Araneda, R.C., Maurer, L.R., Muller, F., and Greer, C.A. (2010).
765 Hyperpolarization-activated cyclic nucleotide-gated channels in olfactory sensory neurons
766 regulate axon extension and glomerular formation. The Journal of neuroscience : the official
767 journal of the Society for Neuroscience *30*, 16498-16508.

768 Mombaerts, P., Wang, F., Dulac, C., Chao, S.K., Nemes, A., Mendelsohn, M., Edmondson, J.,
769 and Axel, R. (1996). Visualizing an olfactory sensory map. Cell *87*, 675-686.

770 Narayana, S.K., Helbig, K.J., McCartney, E.M., Eyre, N.S., Bull, R.A., Eltahla, A., Lloyd, A.R.,
771 and Beard, M.R. (2015). The Interferon-induced Transmembrane Proteins, IFITM1, IFITM2,
772 and IFITM3 Inhibit Hepatitis C Virus Entry. J Biol Chem *290*, 25946-25959.

773 Noyce, R.S., and Richardson, C.D. (2012). Nectin 4 is the epithelial cell receptor for measles
774 virus. Trends Microbiol *20*, 429-439.

775 O'Leary, C.E., Schneider, C., and Locksley, R.M. (2019). Tuft Cells-Systemically Dispersed
776 Sensory Epithelia Integrating Immune and Neural Circuitry. Annu Rev Immunol *37*, 47-72.

777 Ogura, T., Szebenyi, S.A., Krosnowski, K., Sathyanesan, A., Jackson, J., and Lin, W. (2011).
778 Cholinergic microvillous cells in the mouse main olfactory epithelium and effect of acetylcholine
779 on olfactory sensory neurons and supporting cells. J Neurophysiol *106*, 1274-1287.

780 Omura, M., and Mombaerts, P. (2014). Trpc2-Expressing Sensory Neurons in the Main
781 Olfactory Epithelium of the Mouse. Cell Reports *8*, 583-595.

782 Oshimoto, A., Wakabayashi, Y., Garske, A., Lopez, R., Rolen, S., Flowers, M., Arevalo, N., and
783 Restrepo, D. (2013). Potential role of transient receptor potential channel M5 in sensing putative
784 pheromones in mouse olfactory sensory neurons. PLoS One *8*, e61990.

785 Parma, V., Ohla, K., Veldhuizen, M.G., Nim, M.Y., Kelly, C.E., Reed, D.R., Hummel, T.,
786 Munger, S., and Hayes, J.E. (2020). More than just smell - COVID-19 is associated with severe
787 impairment of smell, taste, and chemesthesis. medRxiv, 2020.2005.2004.20090902.

788 Patro, R., Duggal, G., Love, M.I., Irizarry, R.A., and Kingsford, C. (2017). Salmon provides fast
789 and bias-aware quantification of transcript expression. Nature methods *14*, 417-419.

790 Perniss, A., Liu, S., Boonen, B., Keshavarz, M., Ruppert, A.L., Timm, T., Pfeil, U., Soultanova,
791 A., Kusumakshi, S., Delventhal, L.*, et al.* (2020). Chemosensory Cell-Derived Acetylcholine
792 Drives Tracheal Mucociliary Clearance in Response to Virulence-Associated Formyl Peptides.
793 Immunity *52*, 683-699 e611.

794 Petermann, P., Rahn, E., Thier, K., Hsu, M.J., Rixon, F.J., Kopp, S.J., and Knebel-Morsdorf, D.
795 (2015). Role of Nectin-1 and Herpesvirus Entry Mediator as Cellular Receptors for Herpes
796 Simplex Virus 1 on Primary Murine Dermal Fibroblasts. J Virol *89*, 9407-9416.

797 Pyrski, M., Eckstein, E., Schmid, A., Bufe, B., Weiss, J., Chubanov, V., Boehm, U., and Zufall,
798 F. (2017). Trpm5 expression in the olfactory epithelium. Mol Cell Neurosci *80*, 75-88.

799 Pyrski, M., Tusty, M., Eckstein, E., Oboti, L., Rodriguez-Gil, D.J., Greer, C.A., and Zufall, F.
800 (2018). P/Q Type Calcium Channel Cav2.1 Defines a Unique Subset of Glomeruli in the Mouse
801 Olfactory Bulb. Frontiers in Cellular Neuroscience *12*, 295.

802 Quinlan, A.R., and Hall, I.M. (2010). BEDTools: a flexible suite of utilities for comparing
803 genomic features. Bioinformatics *26*, 841-842.

804 Rane, C.K., Jackson, S.R., Pastore, C.F., Zhao, G., Weiner, A.I., Patel, N.N., Herbert, D.R.,
805 Cohen, N.A., and Vaughan, A.E. (2019). Development of solitary chemosensory cells in the
806 distal lung after severe influenza injury. Am J Physiol Lung Cell Mol Physiol *316*, L1141-
807 L1149.

808 Richardson, W.H. (1972). Bayesian-Based Iterative Method of Image Restoration*. J Opt Soc
809 Am *62*, 55-59.

810 Sage, D., Donati, L., Soulez, F., Fortun, D., Schmit, G., Seitz, A., Guiet, R., Vonesch, C., and
811 Unser, M. (2017). DeconvolutionLab2: An open-source software for deconvolution microscopy.
812 Methods *115*, 28-41.

813 Saunders, C.J., Christensen, M., Finger, T.E., and Tizzano, M. (2014). Cholinergic
814 neurotransmission links solitary chemosensory cells to nasal inflammation. Proc Natl Acad Sci U
815 S A *111*, 6075-6080.

816 Sayers, C.L., and Elliott, G. (2016). Herpes Simplex Virus 1 Enters Human Keratinocytes by a
817 Nectin-1-Dependent, Rapid Plasma Membrane Fusion Pathway That Functions at Low
818 Temperature. J Virol *90*, 10379-10389.

819 Sekerkova, G., Zheng, L., Loomis, P.A., Changyaleket, B., Whitlon, D.S., Mugnaini, E., and
820 Bartles, J.R. (2004). Espins are multifunctional actin cytoskeletal regulatory proteins in the
821 microvilli of chemosensory and mechanosensory cells. J Neurosci *24*, 5445-5456.

822 Shestakov, A., Jenssen, H., Nordstrom, I., and Eriksson, K. (2012). Lactoferricin but not
823 lactoferrin inhibit herpes simplex virus type 2 infection in mice. Antiviral Res *93*, 340-345.

824 Shukla, N.D., Tiwari, V., and Valyi-Nagy, T. (2012). Nectin-1-specific entry of herpes simplex
825 virus 1 is sufficient for infection of the cornea and viral spread to the trigeminal ganglia. Mol Vis
826 *18*, 2711-2716.

827 Singh, B.K., Hornick, A.L., Krishnamurthy, S., Locke, A.C., Mendoza, C.A., Mateo, M., Miller-
828 Hunt, C.L., Cattaneo, R., and Sinn, P.L. (2015). The Nectin-4/Afadin Protein Complex and
829 Intercellular Membrane Pores Contribute to Rapid Spread of Measles Virus in Primary Human
830 Airway Epithelia. J Virol *89*, 7089-7096.

831 Singh, B.K., Li, N., Mark, A.C., Mateo, M., Cattaneo, R., and Sinn, P.L. (2016). Cell-to-Cell
832 Contact and Nectin-4 Govern Spread of Measles Virus from Primary Human Myeloid Cells to
833 Primary Human Airway Epithelial Cells. J Virol *90*, 6808-6817.

834 Soneson, C., Love, M.I., and Robinson, M.D. (2015). Differential analyses for RNA-seq:
835 transcript-level estimates improve gene-level inferences. F1000Res *4*, 1521.

836 Tizzano, M., Gulbransen, B.D., Vandenbeuch, A., Clapp, T.R., Herman, J.P., Sibhatu, H.M.,
837 Churchill, M.E., Silver, W.L., Kinnamon, S.C., and Finger, T.E. (2010). Nasal chemosensory
838 cells use bitter taste signaling to detect irritants and bacterial signals. Proc Natl Acad Sci U S A
839 *107*, 3210-3215.

840 Ualiyeva, S., Hallen, N., Kanaoka, Y., Ledderose, C., Matsumoto, I., Junger, W.G., Barrett,
841 N.A., and Bankova, L.G. (2020). Airway brush cells generate cysteinyl leukotrienes through the
842 ATP sensor P2Y2. Science Immunology *5*, eaax7224.

843 Valimaa, H., Tenovuo, J., Waris, M., and Hukkanen, V. (2009). Human lactoferrin but not
844 lysozyme neutralizes HSV-1 and inhibits HSV-1 replication and cell-to-cell spread. Virol J *6*, 53.

845 van der Linden, C., Jakob, S., Gupta, P., Dulac, C., and Santoro, S.W. (2018). Sex separation
846 induces differences in the olfactory sensory receptor repertoires of male and female mice. Nat
847 Commun *9*, 5081.

848 Villar, P.S., Delgado, R., Vergara, C., Reyes, J.G., and Bacigalupo, J. (2017). Energy
849 Requirements of Odor Transduction in the Chemosensory Cilia of Olfactory Sensory Neurons
850 Rely on Oxidative Phosphorylation and Glycolytic Processing of Extracellular Glucose. J
851 Neurosci *37*, 5736-5743.

852 von Moltke, J., Ji, M., Liang, H.E., and Locksley, R.M. (2016). Tuft-cell-derived IL-25 regulates
853 an intestinal ILC2-epithelial response circuit. Nature *529*, 221-225.

854 Wu, Y., Ma, L., Duyck, K., Long, C.C., Moran, A., Scheerer, H., Blanck, J., Peak, A., Box, A.,
855 Perera, A.*, et al.* (2018). A Population of Navigator Neurons Is Essential for Olfactory Map
856 Formation during the Critical Period. Neuron *100*, 1066-1082 e1066.

857 Yamaguchi, T., Yamashita, J., Ohmoto, M., Aoude, I., Ogura, T., Luo, W., Bachmanov, A.A.,
858 Lin, W., Matsumoto, I., and Hirota, J. (2014). Skn-1a/Pou2f3 is required for the generation of
859 Trpm5-expressing microvillous cells in the mouse main olfactory epithelium. BMC Neurosci *15*,
860 13.

861 Yamashita, J., Ohmoto, M., Yamaguchi, T., Matsumoto, I., and Hirota, J. (2017). Skn-1a/Pou2f3
862 functions as a master regulator to generate Trpm5-expressing chemosensory cells in mice. PLoS
863 One *12*, e0189340.

864 Yan, C.H., Faraji, F., Prajapati, D.P., Boone, C.E., and DeConde, A.S. (2020a). Association of
865 chemosensory dysfunction and Covid-19 in patients presenting with influenza-like symptoms.
866 Int Forum Allergy Rhinol.

867 Yan, C.H., Faraji, F., Prajapati, D.P., Ostrander, B.T., and DeConde, A.S. (2020b). Self-reported
868 olfactory loss associates with outpatient clinical course in Covid-19. Int Forum Allergy Rhinol.

869 Yang, J., Zhu, X., Liu, J., Ding, X., Han, M., Hu, W., Wang, X., Zhou, Z., and Wang, S. (2012).
870 Inhibition of Hepatitis B virus replication by phospholipid scramblase 1 in vitro and in vivo.
871 Antiviral Res *94*, 9-17.

872 Yu, J., Li, M., Wilkins, J., Ding, S., Swartz, T.H., Esposito, A.M., Zheng, Y.M., Freed, E.O.,
873 Liang, C., Chen, B.K.*, et al.* (2015). IFITM Proteins Restrict HIV-1 Infection by Antagonizing
874 the Envelope Glycoprotein. Cell Rep *13*, 145-156.

875 Zerbino, D.R., Achuthan, P., Akanni, W., Amode, M.R., Barrell, D., Bhai, J., Billis, K.,
876 Cummins, C., Gall, A., Giron, C.G.*, et al.* (2018). Ensembl 2018. Nucleic Acids Res *46*, D754-
877 D761.

878 Zhang, Y., Hoon, M.A., Chandrashekar, J., Mueller, K.L., Cook, B., Wu, D., Zuker, C.S., and
879 Ryba, N.J. (2003). Coding of sweet, bitter, and umami tastes: different receptor cells sharing
880 similar signaling pathways. Cell *112*, 293-301.

881 Zheng, Y., Qin, Z., Ye, Q., Chen, P., Wang, Z., Yan, Q., Luo, Z., Liu, X., Zhou, Y., Xiong, W.*,*
882 *et al.* (2014). Lactoferrin suppresses the Epstein-Barr virus-induced inflammatory response by
883 interfering with pattern recognition of TLR2 and TLR9. Lab Invest *94*, 1188-1199.

884 Zheng, Y., Zhang, W., Ye, Q., Zhou, Y., Xiong, W., He, W., Deng, M., Zhou, M., Guo, X.,
885 Chen, P.*, et al.* (2012). Inhibition of Epstein-Barr virus infection by lactoferrin. J Innate Immun
886 *4*, 387-398.

887 Ziegler, C.G.K., Allon, S.J., Nyquist, S.K., Mbano, I.M., Miao, V.N., Tzouanas, C.N., Cao, Y.,
888 Yousif, A.S., Bals, J., Hauser, B.M., *et al.* (2020). SARS-CoV-2 receptor ACE2 is an interferon-
889 stimulated gene in human airway epithelial cells and is detected in specific cell subsets across
890 tissues. Cell.
891
892

Name	OSN_eGFP-	OSN_eGFP+	MVC_eGFP	p-value adjusted
Olfr292	3.61	959	4.29	6.35E-09
Olfr282	2.05	486	0	8.01E-05
Olfr1434	53.3	7730	0	9.71E-16
Olfr390	101	10800	43.1	1.56E-16
Olfr305	6.14	612	0	6.3E-12
Olfr293	6.96	664	16.9	1.42E-07
Olfr378	3.41	322	0	1.1E-06
Olfr128	39.6	3660	12.7	7.33E-14
Olfr344	16.2	1050	0	1.4E-11
Olfr307	7.59	393	0	3.76E-06
Olfr391	156	8000	9.79	1.01E-15
Olfr299	13.1	651	0	4.58E-09
Olfr142	36.4	1720	3.77	1.62E-08
Olfr1	147	5720	52.7	3.08E-10
Olfr1279	16.4	552	10.9	3.52E-07
Olfr39	13.8	388	21	2.81E-06
Olfr1447	64.1	1610	0	1.23E-07
Olfr728	2150	45700	320	6.13E-22
Olfr727	560	11000	179	1.64E-07
Olfr1555-ps1	10.1	175	0	0.0397
Olfr346	27.6	465	0	3.85E-05
Olfr1228	533	5320	35.4	3.09E-08
Olfr1181	87.4	766	4.61	0.000766
Olfr943	97.1	844	2.89	0.000886
Olfr298	60.1	509	0	0.00132

Table 1. Levels of expression and adjusted p-value for the olfactory receptor genes whose levels are significantly higher in OSN_eGFP+ compared to OSN_eGFP-. These olfactory receptors had an adjusted p-value for expression level difference between OSN_eGFP+ compared to OSN_eGFP- and had a fold change > 4 and average expression > 100 counts.

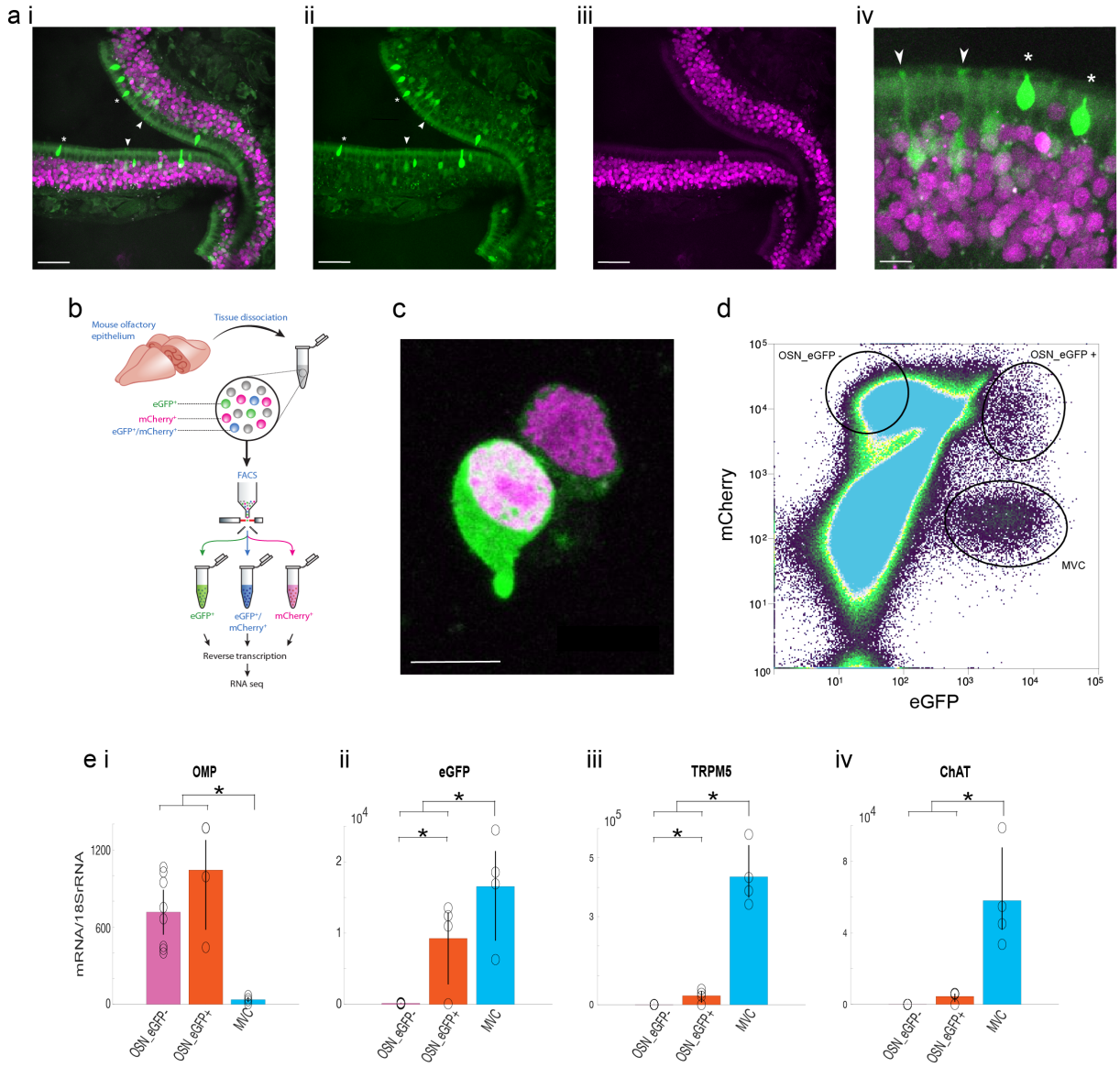

Figure 1. Fluorescence activated sorting (FACS) of cells isolated from the olfactory epithelium.

a. TRPM5 promoter driven expression of eGFP and OMP promoter driven expression of mCherry in the olfactory epithelium. Expression of eGFP is found both in MVCs that do not express mCherry (asterisk) and in OSNs double labeled with eGFP and mCherry (arrow). **i.**

908 Composite, **ii.** eGFP, **iii.** mCherry, **iv**. Composite magnification. Magenta: mCherry, green:
909 eGFP. Scale bar: i-iii, 50 μm, iv, 10 μm.
910 **b.** Schematic of RNA-seq process from tissue to RNA extraction. Mouse OE was dissociated
911 into single cells and sorted via FACS. RNA was extracted from each of the resulting cell
912 populations.
913 **c.** Two isolated OSNs differing in eGFP expression. Magenta: mCherry, green: eGFP. Scale bar:
914 10 μm.
915 **d.** Distribution of mCherry and eGFP fluorescence intensity for FACS-sorted cells. Three cell
916 populations were isolated for RNAseq: Cells with low OMP promoter-driven mCherry
917 expression and high TRPM5 promoter-driven eGFP expression (MVC_eGFP cells), cells with
918 high OMP promoter-driven mCherry and low eGFP expression (OSN_eGFP- cells) and cells
919 with eGFP expression of the same magnitude as MVC_eGFP cells and high OMP promoter-
920 driven mCherry expression (OSN_eGFP+ cells). The number of cells collected for this FACS
921 run were: OSN_eGFP-s 1,500,000, OSN_eGFP+s 5336 and MVC_eGFP cells 37,178.
922 **e.** qPCR levels (normalized to levels 18s RNA) for expression of transcripts encoding for OMP
923 (**i**), TRPM5 (**ii**), eGFP (**iii**) and ChAT (**iv**). The asterisks denote significant differences tested
924 with either t-test or ranksum with p-values below the significance p-value corrected for multiple
925 comparisons using the false discovery rate (pFDR)(Curran-Everett, 2000). pFDR is 0.033 for
926 OMP, 0.05 for TRPM5, 0.05 for eGFP and 0.03 for ChAT, n=8 for OMP OSN_eGFP-s, 4 for
927 OMP OSN_eGFP+s and 4 for MVC_eGFP cells.
928
929

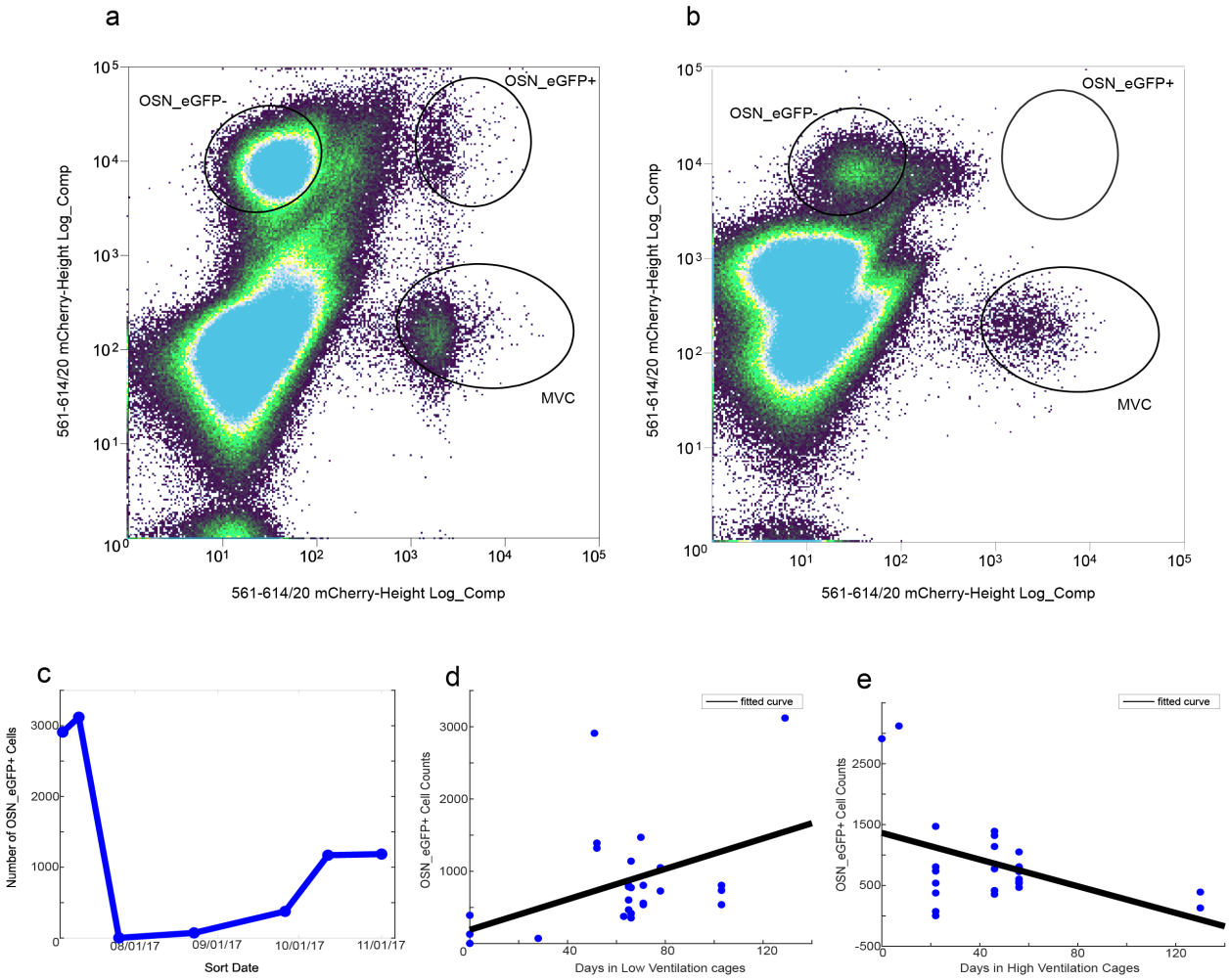

Figure 2. Decreased yield of OSN_eGFP+ cells when mice are moved from low ventilation (LV) to high ventilation (HV) cages.

a and b. Distribution of mCherry and eGFP fluorescence intensity for FACS-sorted cells that either were not transferred to HV cages (**a**) or were transferred to HV cages for 22 days before sorting (**b**).

c. Time course showing change in the number of sorted OSN_eGFP+s after mice were transferred to HV cages.

d and e. Dependence of the yield of OSN_eGFP+ cells after sorting on the number of days in LV cages (**d**) or the number of days in HV cages (**e**).

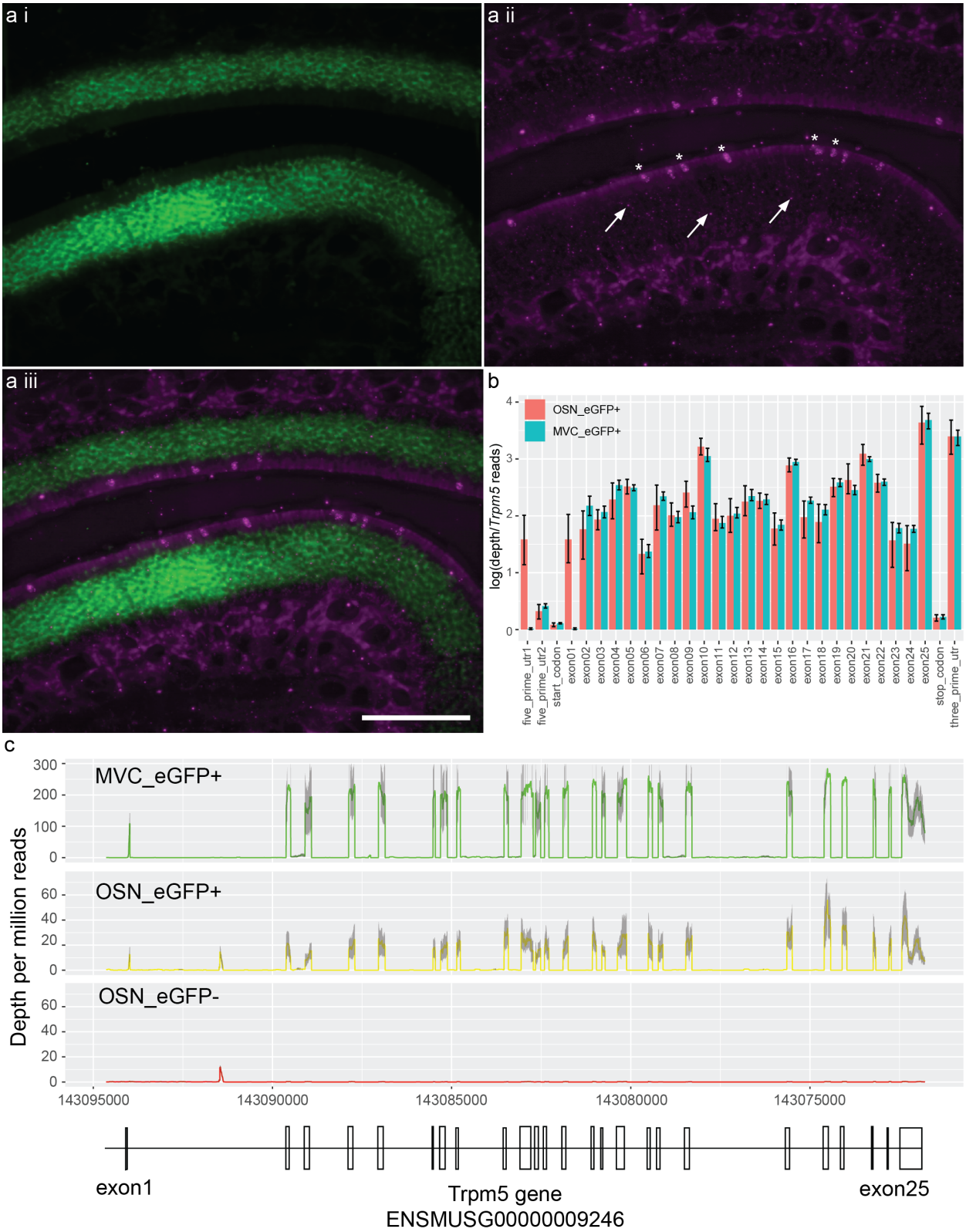
a i
a ii
a iii
b
OSN_eGFP+
MVC_eGFP+
log(depth/Trpm5 reads)
five_prime_utr1
five_prime_utr2
start_codon
exon01
exon02
exon03
exon04
exon05
exon06
exon07
exon08
exon09
exon10
exon11
exon12
exon13
exon14
exon15
exon16
exon17
exon18
exon19
exon20
exon21
exon22
exon23
exon24
exon25
stop_codon
three_prime_utr
c
MVC_eGFP+
OSN_eGFP+
OSN_eGFP-
Depth per million reads
143095000
143090000
143085000
143080000
143075000
exon1
Trpm5 gene
ENSMUSG00000009246
exon25

942 **Figure 3. Coverage of TRPM5 transcript by RNAseq in the different cell groups sorted**
943 **from the olfactory epithelium**
944 **a.** In situ for TRPM5 and OMP transcripts in the olfactory epithelium shows strong label for
945 TRPM5 in MVCs (asterisks) and sparse labeling in the OSN nuclear layer (arrows). **i.** OMP, **ii.**
946 TRPM5, **iii.** Composite. The scale bar is 100 μm.
947 **b and c.** Coverage of the reads for the TRPM5 transcript for the different cell groups. Read
948 coverage was computed with 'Samtools depth' over the region corresponding to the Trpm5 gene.
949 **b.** Coverage per exon. All samples normalized to TRPM5 reads show distribution among exons
950 with little difference between MVC and OSN_eGFP+ cells.
951 **c.** Coverage shown per base pair as a function of location in the genomic DNA. Plots show read
952 depth per base pair for each cell type normalized to total number of mapped reads. Gray shading
953 indicates 95% confidence interval.
954

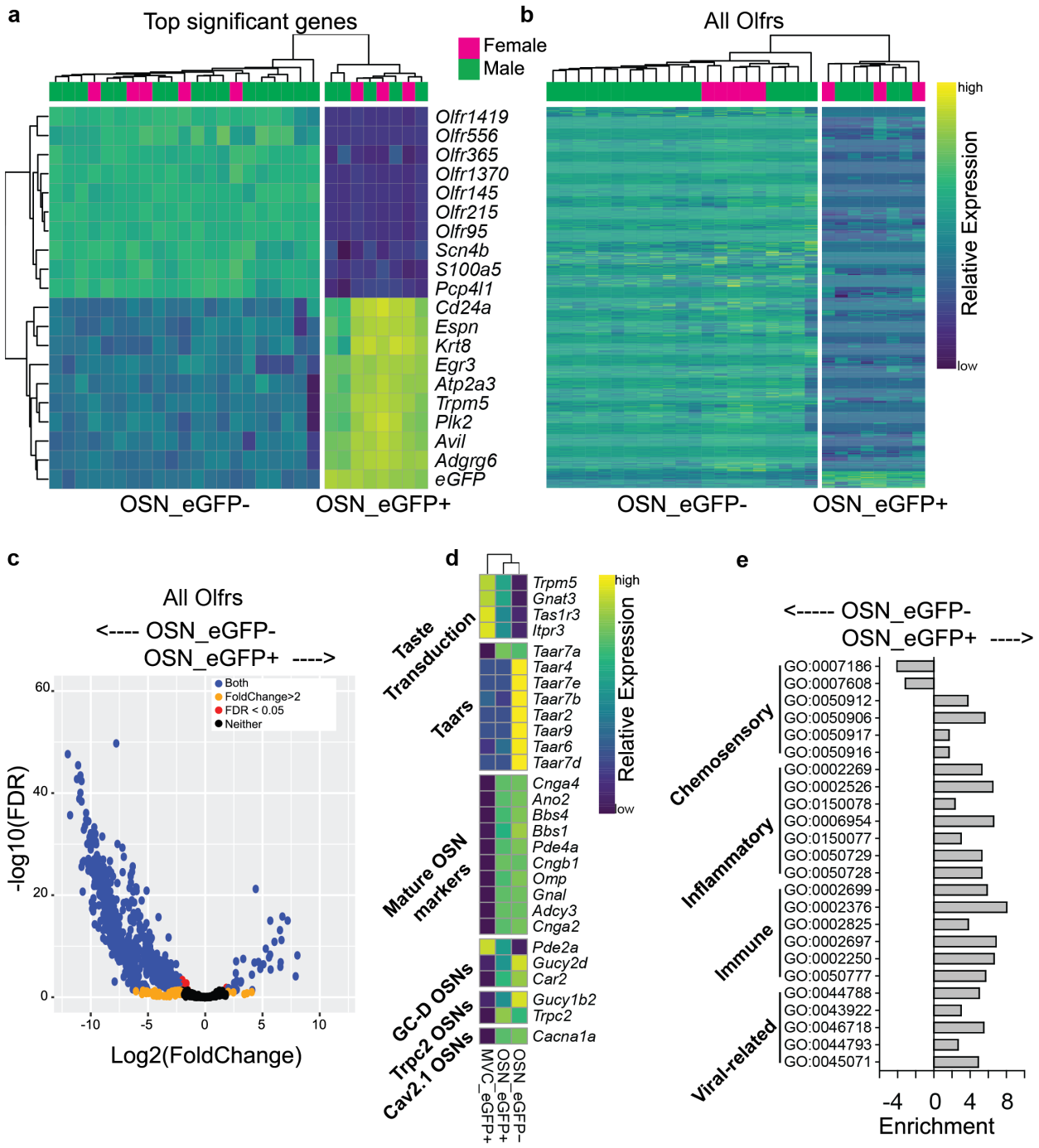

Figure 4. RNAseq comparison of OSN_eGFP- and OSN_eGFP+ cells.

a. Heatmap showing the top 10 upregulated and top 10 downregulated genes identified by DESeq2.

b. Heatmap showing all *Olfr* genes detected in the data.

960 For both a and b, row and column order were determined automatically by the *pHeatmap*
961 package in R. For each data point relative expression was calculated by subtracting the average
962 row value from each individual value.
963 **c.** Volcano plot of all Olfactory receptors, demonstrating the small number of enriched olfactory
964 receptors in the OSN_eGFP+ population.
965 **d.** Hierarchical clustering of transcripts for taste transduction and transcripts expressed in
966 canonical and non-canonical OSNs identified by RNAseq as significantly different in expression
967 between the cell groups. We compared expression of transcripts involved in taste transduction,
968 canonical olfactory transduction, and non-canonical OSNs. The non-canonical OSNs considered
969 here included guanilyl-cyclase D (GC-D) OSNs (Juilfs et al., 1997), Trpc2 OSNs (Omura and
970 Mombaerts, 2014), Cav2.1 OSNs (Pyrski et al., 2018), and OSNs expressing trace amine-
971 associated receptors (Taars) (Liberles, 2015). Transcripts identified by DESeq2.
972 **e.** Gene ontology (GO) term enrichment was calculated from differentially expressed genes using
973 *TopGO* in R. An enrichment value for genes with Fischer p value <0.05 was calculated by
974 dividing the number of expressed genes within the GO term by the number expected genes (by
975 random sampling, determined by *TopGO*).
976
977
978

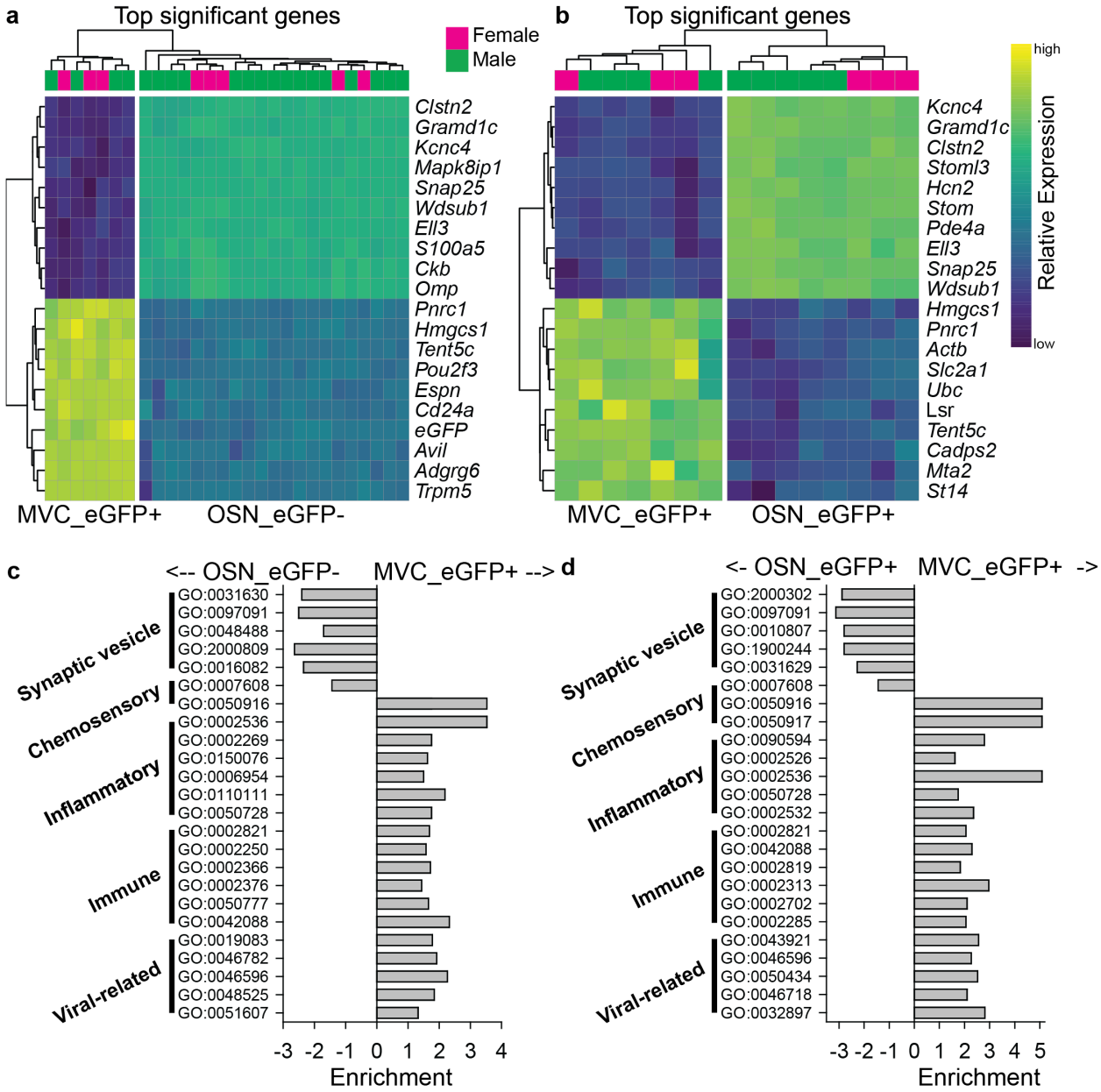

Figure 5. RNAseq comparison of OSN_eGFP- and OSN_eGFP+ vs. MVC_eGFP cells. **a and b.** Heatmaps showing hierarchical clustering of the top 10 upregulated and top 10 downregulated genes identified by DESeq2. **a.** OSN_eGFP- vs. MVC_eGFP cells. **b**. OSN_eGFP+ vs. MVC_eGFP cells. For both a and b, row and column order were determined automatically by the *pHeatmap* package in R. For each data point relative expression was calculated by subtracting the average row value from each individual value.

986 **c and d.** Gene ontology (GO) term enrichment was calculated from differentially expressed
987 genes using *TopGO* in R. **c.** OSN_eGFP- vs. MVC_eGFP cells. **d**. OSN_eGFP+ vs.
988 MVC_eGFP cells. An enrichment value for genes with Fischer p value <0.05 was calculated by
989 dividing the number of expressed genes within the GO term by the number expected genes (by
990 random sampling, determined by *TopGO*).
991
992

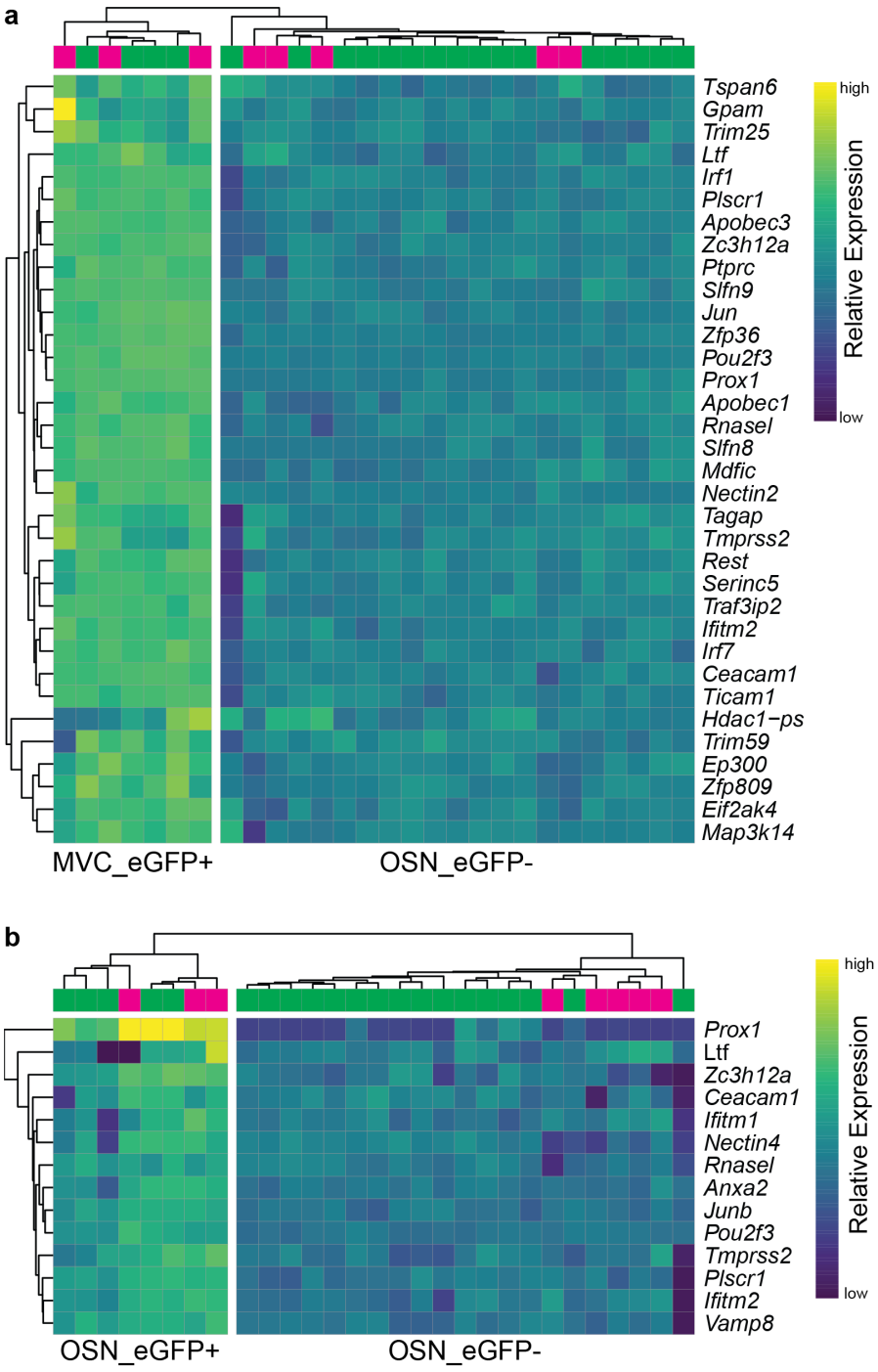

Figure 6. Significant differences in virally-related gene ontology. Heatmaps show hierarchical clustering of significantly differentially expressed genes identified by DESeq2. **a.** MVC_eGFP cells compared to OSN_eGFP-. **b.** OSN_eGFP+ compared to OSN_eGFP-.

998 **Supplemental Information**

999

1000

1001 **Transcriptional profiling reveals TRPM5-expressing cells involved in viral infection in the**

1002 **olfactory epithelium**

1003

1004 B. Dnate' Baxter[1,2,‡], Eric D. Larson[3 ‡], Paul Feinstein[4], Arianna Gentile Polese[1,2], Andrew N.

1005 Bubak[5], Christy S. Niemeyer[5], Laetitia Merle[1,2], Doug Shepherd[6], Vijay R. Ramakrishnan[3],

1006 Maria A. Nagel[5], and Diego Restrepo[1,2,*]

1007

1008

1009 **Figure 4 – figure supplement 1. Excel worksheet with the results of comparison of gene**

1010 **transcription between OSN_EGFP+ and OSN_EGFP-.**

1011

1012 **Figure 4 – figure supplement 2. Metadata for the RNAseq.**

1013

1014 **Figure 5 - figure supplement 1. Excel worksheet with the results of comparison of gene**

1015 **transcription between MVC_eGFP cells and OSN_EGFP-.**

1016

1017 **Figure 5 - figure supplement 2. Excel worksheet with the results of comparison of gene**

1018 **transcription between MVC_eGFP cells and OSN_EGFP+.**

1019

1020

1021

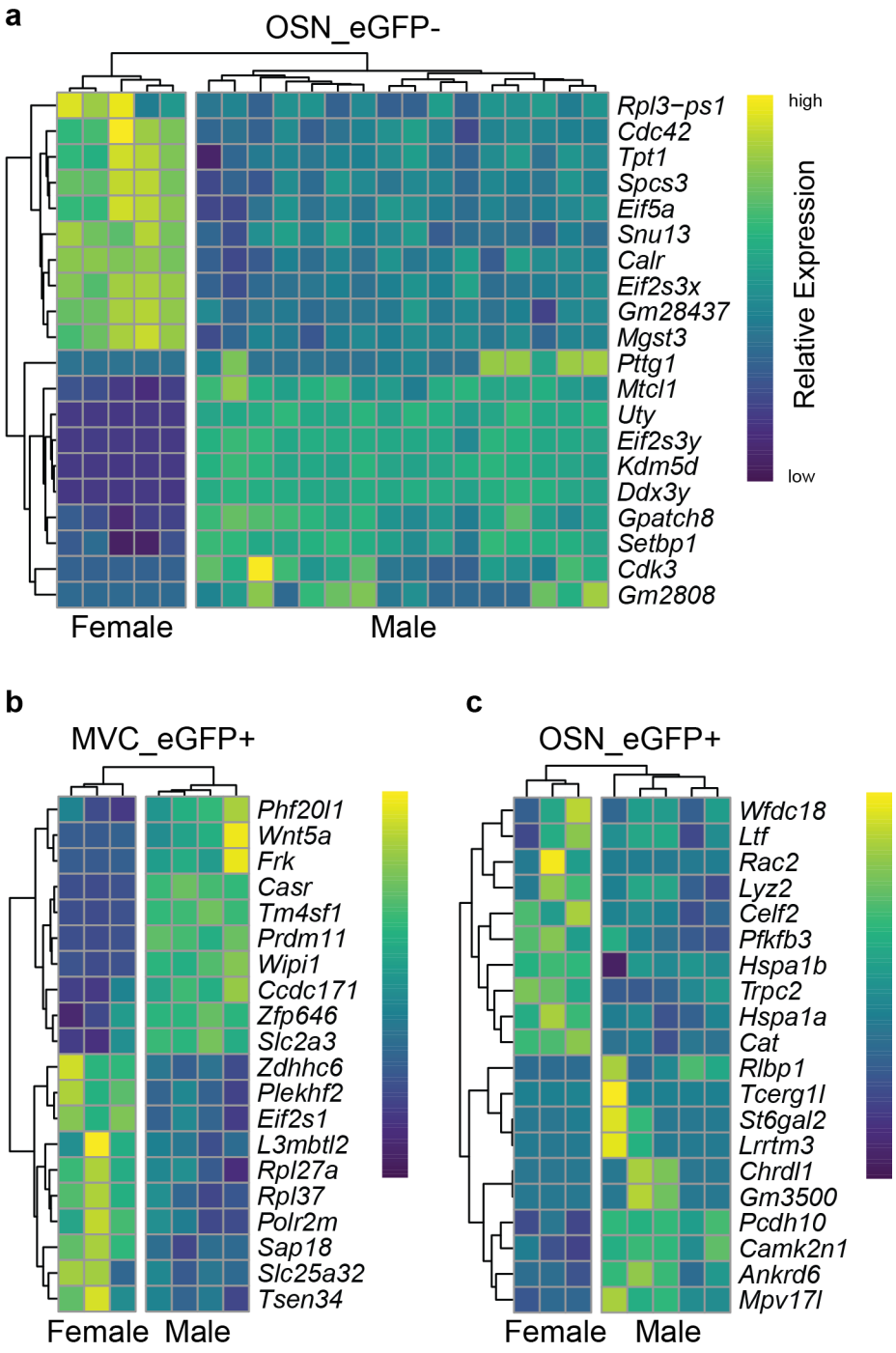

Figure 5 – figure supplement 3. Hierarchical clustering of transcripts identified by RNAseq as significantly differentially expressed between male and female. a. OSN_eGFP-. **b.** MVC_eGFP cells **c.** OSN_eGFP+. Transcripts identified by DESeq2.

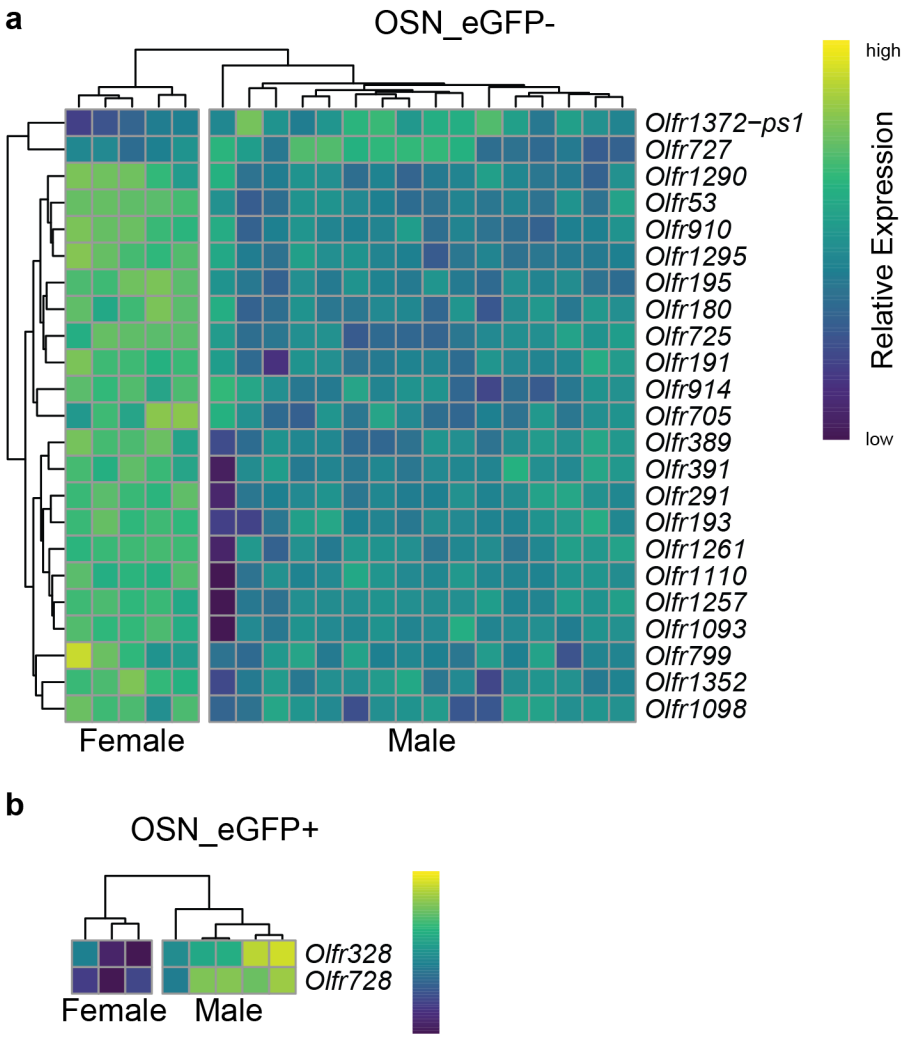

Figure 5 – figure supplement 4. Hierarchical clustering of olfactory receptor transcripts identified by RNAseq as significantly differentially expressed between male and female. a. OSN_eGFP-. **b.** OSN_eGFP+. Transcripts identified by DESeq2.

1032 **Figure 6 – figure supplement 1. Excel worksheet with the results of gene ontology**

1033 **enrichment analysis for OSN_eGFP+ compared to OSN_eGFP-.**

1034

1035 **Figure 6 - figure supplement 2. Excel worksheet with the results of gene ontology**

1036 **enrichment analysis for MVC_eGFP cells compared to OSN_EGFP-.**

1037

1038 **Figure 6- figure supplement 3. Excel worksheet with the results of gene ontology**

1039 **enrichment analysis for MVC_eGFP cells compared to OSN_EGFP+.**

1040

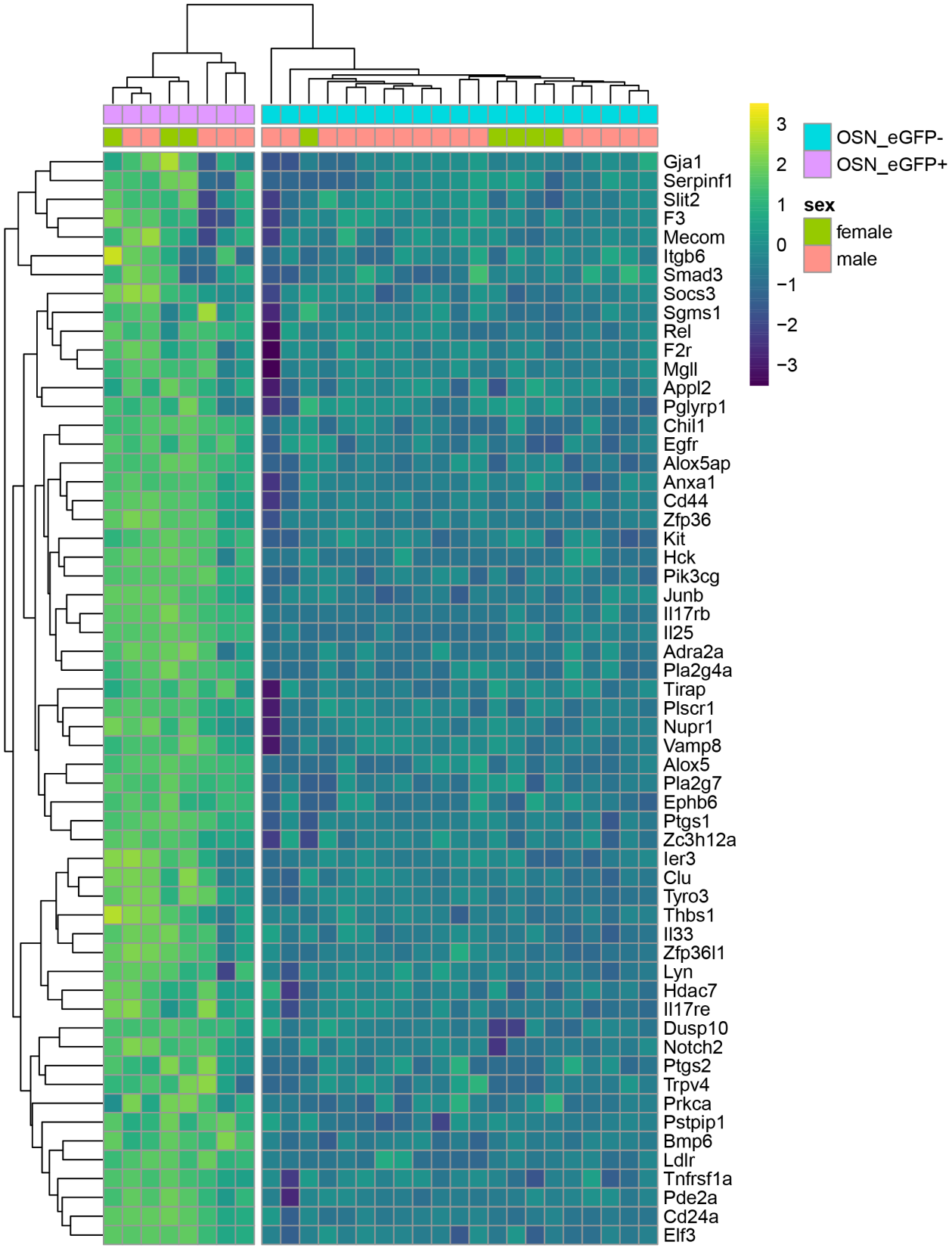
Gja1
Serpinf1
Slit2
F3
Mecom
Itgb6
Smad3
Socs3
Sgms1
Rel
F2r
Mgll
Appl2
Pglyrp1
Chil1
Egfr
Alox5ap
Anxa1
Cd44
Zfp36
Kit
Hck
Pik3cg
Junb
Il17rb
Il25
Adra2a
Pla2g4a
Tirap
Plscr1
Nupr1
Vamp8
Alox5
Pla2g7
Ephb6
Ptgs1
Zc3h12a
Ier3
Clu
Tyro3
Thbs1
Il33
Zfp36l1
Lyn
Hdac7
Il17re
Dusp10
Notch2
Ptgs2
Trpv4
Prkca
Pstpip1
Bmp6
Ldlr
Tnfrsf1a
Pde2a
Cd24a
Elf3
3
2
1
0
−1
−2
−3
OSN_eGFP-
OSN_eGFP+
sex
female
male

1041

1042 **Figure 6- figure supplement 4. Significant differences in inflammation gene ontology for**

1043 **OSN_eGFP+ compared to OSN_eGFP-.**

1044

OSN_eGFP-
MVC_eGFP+
sex
female
male
3
2
1
0
−1
−2
−3
Rell2
Zfp365
Lynx1
Rell1
Rora
Tcirg1
Gja1
Sgms1
Sulf1
Tnip2
Relt
Hdac7
Serpina3n
Nupr1
Mgll
Reg3g
F3
Pglyrp1
F2r
Tnfaip3
Tgfb2
Vamp8
Ccn3
Tirap
Plscr1
Rel
Itgav
Il17re
Mdk
Mif
Il1rap
Prcp
Adora1
Tnip1
Bcor
Itgb6
Gprc5b
Sall1
Pstpip1
Clu
Tnfrsf1a
Chst2
Gstp1
H2−T23
Smad3
Kit
Hck
Pik3cg
Pde2a
Cd24a
Lyn
Serpinf1
Anxa11
Il4ra
Ldlr
Zfp36l2
Elf3
Jun
Junb
Adra2a
Il17rb
Il25
Jund
Pdcd4
Pla2g4a
Appl2
Anxa1
Cd44
Zfp36
Ephb6
Nfkbiz
Ptgs1
Zc3h12a
Nr1d1
Ceacam1
Pla2g7
Thbs1
Adrb2
Chil1
Bmp7
Egfr
Socs3
Ticam1
Stat5a
Ptgs2
Nfkbia
Thrb
Mecom
Notch1
Slit2
Stap1
Ets1
Ier3
Prkca
Alox5
Zfp36l1
Trpv4
Alox5ap
Tyro3
Relb
Uaca
Parp4
Ano6
Sbno2
Dusp10
Notch2
Ndst1
Snap23

1045

1046 **Figure 6- figure supplement 5. Significant differences in inflammation gene ontology for**

1047 **MVC_eGFP+ compared to OSN_eGFP-.**

1048

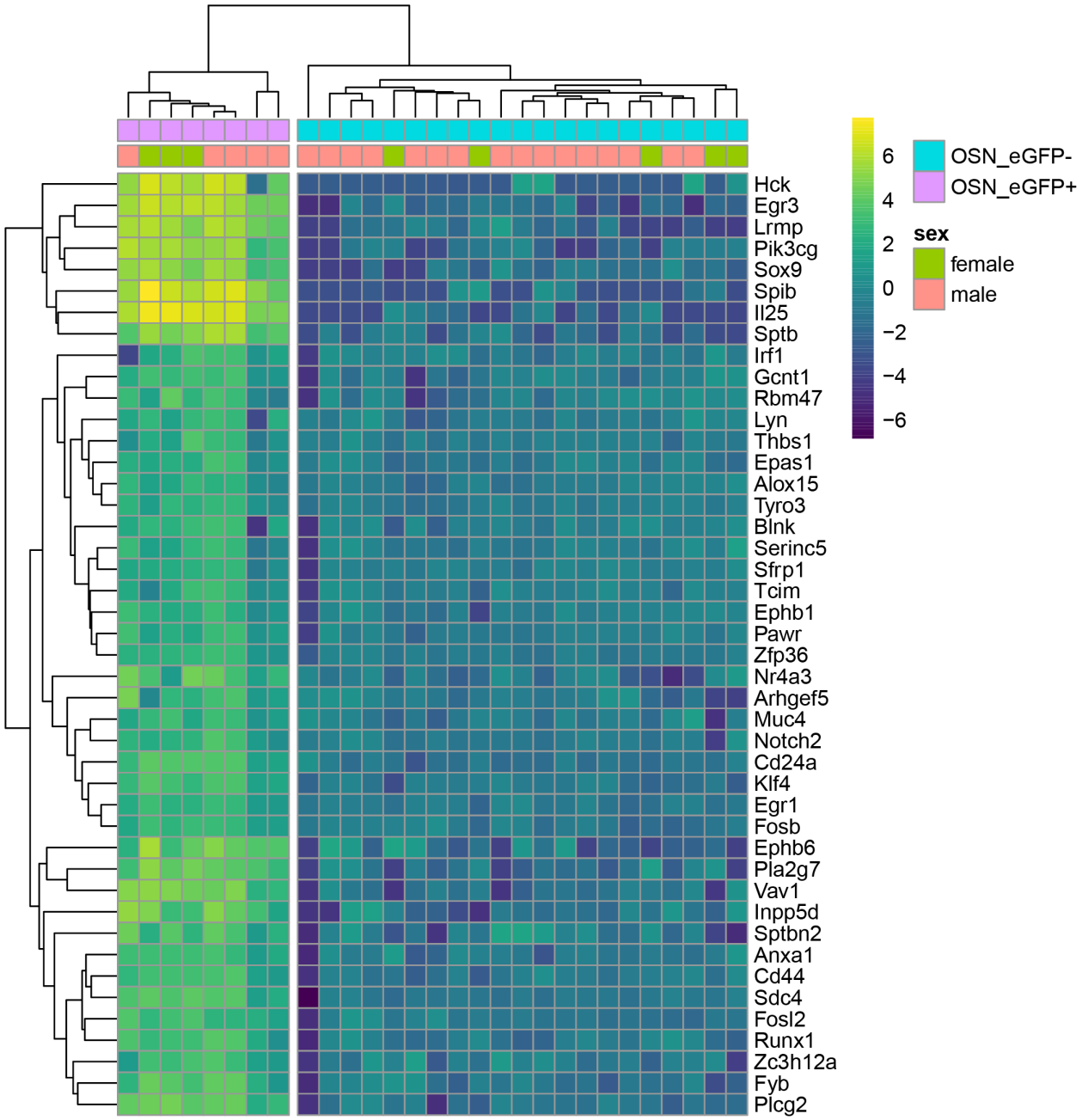

Figure 6- figure supplement 6. Significant differences in immune gene ontology for OSN_eGFP+ compared to OSN_eGFP-.

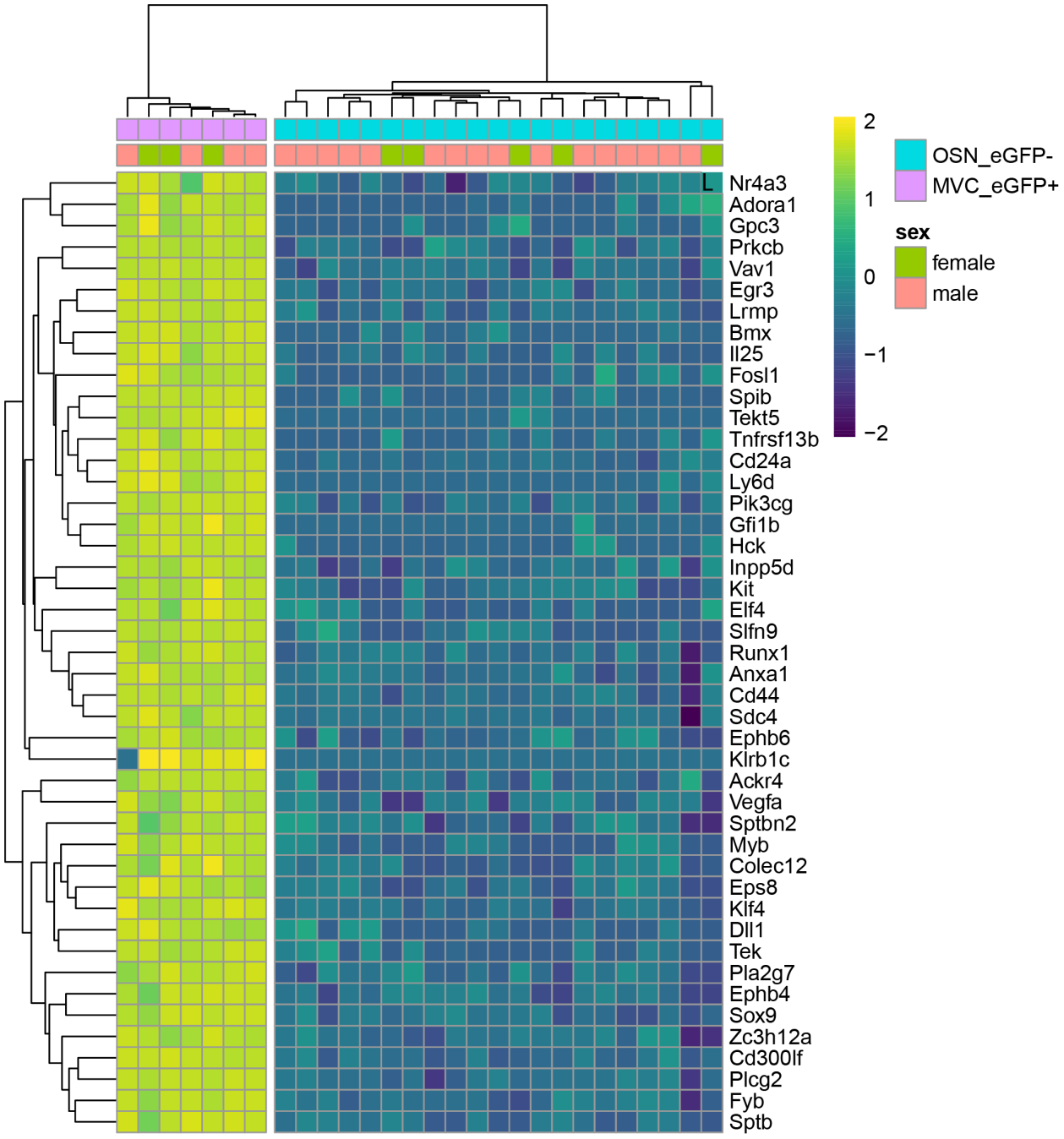

Figure 6- figure supplement 7. Significant differences in immune gene ontology for MVC_eGFP+ compared to OSN_eGFP-.